Constraining the age of superimposed glacial records in mountain environments with multiple dating methods (Cantabrian Mountains, Iberian Peninsula)

Laura Rodríguez-Rodríguez[a], **María José Domínguez-Cuesta**[b], **Vincent Rinterknecht**[a], **Montserrat Jiménez-Sánchez**[b], **Saúl González-Lemos**[b], **Laëtitia Léanni**[c], **Jorge Sanjurjo**[d], **Daniel Ballesteros**[e], **Pablo Valenzuela**[b], **Sergio Llana-Fúnez**[b], **ASTER Team**[c]

[a] *Laboratoire de Géographie Physique (UMR 8591), Centre National de la Recherche Scientifique, 1 place Aristide Briand, FR-92195 Meudon (CEDEX), France. E-mail: (corresponding author)*

[b] *Departamento de Geología, Universidad de Oviedo, Arias de Velasco s/n, 33005 Oviedo, Spain*

[c] *Aix Marseille Université, CNRS, IRD, INRA, Coll France, UM34 CEREGE, Technopôle de l'Environnement Arbois-Méditerranée, BP80,13545 Aix-en-Provence, France [ASTER Team: Georges Aumaître, Didier Bourlès, Karim Keddadouche]*

[d] *Instituto Universitario de Xeoloxía Isidro Parga Pondal, Universidade da Coruña. Castro de Elviña s/n, 15008 A Coruña, Spain*

[e] *IDEES UMR 6266, Université de Rouen-Normandie and CNRS, Mount Saint-Aignan, CEDEX, France.*

Abstract

Numerous cases of timing differences between glacier advances recorded in mountain environments have been documented over the last decade, usually suggesting potential age conflicts between the different dating techniques. The frequent use of a single technique to date numerically a given glacial sequence makes it difficult to address to

what extent age differences can be an artifact related to biased numerical age results or a paleoclimate signature. Here we present a new set of 43 numerical ages based on three dating techniques —[10]Be surface exposure dating; radiocarbon; and optically stimulated luminescence— that complement the chronology of Pleistocene glacial advances in the Porma valley, in the central Cantabrian Mountains of Spain. Results compliment previous chronologies in the area, supporting an important glacial advance during Marine Isotope Stage 3 (Stage IIa: ~56 ka) that culminated with the Last Glacial Maximum advance (Stage IIb: ~33–24 ka) of MIS 2 in response to increased rainfall and solar insolation minima. Glacier fronts reached elevations as low as 1130 m a.s.l. possibly without overriding evidence related to the previous Pleistocene glacial maximum extent. Glacier recession in the Cantabrian Mountains started at 21–20 ka ago, after the global LGM. We suggest that the recession was initiated by increased insolation followed by hyper-cool and dry conditions during Heinrich Stadial 1 in response to meltwater discharges in the North Atlantic.

Key words

[10]Be surface exposure dating; radiocarbon; optically stimulated luminescence; Last Glacial Maximum; Cantabrian Mountains; Iberian Peninsula; Glaciation.

1. Introduction

Formerly glaciated landscapes have been a frequent research topic in the last decades to understand the timing, extent, and behavior of Quaternary glaciations with regards of past climate change and atmospheric circulation patterns. However, as glacial chronologies grow in number more cases of asynchrony in glacier behavior have been detected around the world for the Last Glacial Cycle, evidencing the limited chronostratigraphical value of some broadly used correlation terms such as the Last Glacial Maximum or LGM (c. 23–19 ka) (Hughes et al., 2013). A recent study proposes new limiting ages for the global

LGM event of 27.5–23.3 ka, comprising the peak dust concentration in the polar ice cores, the global sea-level minima, and both the coldest and driest part of the Last Glacial Cycle and the peak in global ice volume (Hughes and Gibbard, 2015).

The timing differences between glacier fluctuations recorded in the different mountain ranges across South Europe and the Mediterranean region received special attention due to age conflicts found between Cosmic Ray Exposure (CRE) chronologies and those derived from other techniques like Optically Stimulated Luminescence (OSL) and radiocarbon (Hughes and Woodward, 2008). In one hand, CRE chronologies supported extensive mountain glacier advances during the so-called LGM of Marine Isotope Stage 2 (MIS 2) in the Eastern Alps (Ivy-Ochs et al., 2008); the Carpathians (Makos et al., 2018); most mountain areas of the Anatolian Peninsula (Akçar et al., 2014, Sarıkaya et al., 2014); the Sistema Central in Iberia (Carrasco et al., 2015, Carrasco et al., 2011, Palacios et al., 2012a, Palacios et al., 2012b, Palacios et al., 2011); and some Pyrenean valleys (Pallàs et al., 2006, Delmas et al., 2008, Palacios et al., 2015). On the other hand, analyses relying on alternative dating techniques (U-Th, radiocarbon, OSL) pointed out to ages older than the LGM of MIS 2 for the most extensive glacial advance locally recorded in areas such as the Swiss Alps (Dehnert et al., 2010); the Pindus Mountains (Hughes et al., 2006, Woodward and Hughes, 2011); the coastal mountains of the Adriatic Sea (Hughes et al., 2010); the Apennines (Giraudi et al., 2011); or the Cantabrian Mountains (Jiménez-Sánchez and Farias-Arquer, 2002, Serrano et al., 2012, Frochoso et al., 2013, Jiménez-Sánchez et al., 2013). In the Iberian Peninsula, only a limited number of sites in the Pyrenees (Pallàs et al., 2010, Delmas et al., 2011) and the Cantabrian Mountains (Vidal Romaní et al., 1999, Rodríguez-Rodríguez et al., 2016) have provided CRE chronologies compatible with a Pleistocene glacial maximum older than the LGM of MIS 2. Timing asynchronies may have paleoclimate significance (Calvet, 2012, Calvet

et al., 2011), but can also be an artifact related to the use of different dating techniques applied to samples of diverse nature and context with regards of the glacial environment (Hughes et al., 2013). However, since most local chronologies are relying on a single dating technique, it is difficult to assess which dating method may be providing the most accurate chronology in a particular study area. Here we used three among the most frequently employed techniques in the literature: [10]Be CRE, radiocarbon, and OSL, to date the glacial record preserved in a single glacier catchment and to cross-compare the obtained results.

Our study focuses on the Porma catchment, located on the southern slope of the central Cantabrian Mountains that extend along the northern coast of the Iberian Peninsula. Along the coast the maritime climate is strongly influenced by the North Atlantic Ocean (Fig. 1). In the Porma catchment, a previous set of 27 dated samples taken from glacial erratics and moraines support a local Pleistocene glacial maximum coeval with MIS 5d (minimum [10]Be CRE age of 113.9 ± 7.1 ka, based on boulders ages from MUR, LIL and CEL sites) and a subsequent glacial advance of similar extent during MIS 4 (minimum [10]Be CRE age of 55.7 ± 4.0 ka, based on boulders from RED, LIL and CEL sites) (Rodríguez-Rodríguez et al., 2016). In addition, a limited number of boulders from the LIL composite moraine suggests a possible of a re-advance of the Porma glacier during MIS 2, at the same time as the growth of continental ice sheets to their maximum LGM positions (Clark et al., 2009). In favor of this hypothesis, a group of glacial erratics sampled on top of the Loma Fondría ice-moulded surface (FRIA samples) placed the beginning of the last glacial retreat at a minimum [10]Be CRE age of 17.7 ± 1.0 ka (n=5), which is consistent with the minimum [10]Be CRE age of 15.7 ± 0.8 ka (n=5) obtained for the foremost ridge of a rock glacier (REQ samples) at 1620 m a.s.l. Additionally, a previous palynology study carried in a peat bog deposited in a glacially over-deepened

depression close to the San Isidro Pass provided a ^{14}C age of 9570 ± 200 yr BP at a depth of 775 to 780 cm (Fombella-Blanco et al., 2003, Fombella-Blanco et al., 2004). Calibrated with Calib Rev 7.0.2 using IntCal13 (Stuiver and Reimer, 1993, Reimer et al., 2013), it provides a minimum age of 10.3–11.4 cal ka BP (2σ interval) and suggests glacier retreat from this area at the beginning of the Holocene. On the northern slopes of the central Cantabrian Mountains, the sequence of recessional moraines dated in the nearby Monasterio valley (BRA-VAL samples in the north slope of the range) yield minimum [10]Be CRE ages in the range 18.1–16.7 ka that are equally consistent with glacier retreat after the LGM of MIS 2 (Rodríguez-Rodríguez et al., 2017). Based on the preexisting datasets, we have performed new [10]Be CRE analyses on twenty samples taken from lateral and recessional moraines along the Porma valley and its main tributaries to check our hypothesis that glaciers remained close to their maximum extent position during the LGM of MIS 2. Additionally, we report sixteen radiocarbon and seven OSL ages obtained on glacial, glacial-related and post-glacial deposits to cross-check if timing asynchronies exist between the results of the different dating techniques and to discuss eventually their possible causes.

Figure 1.- (A) Location of the study area in the context of the North Atlantic region [trajectory of the main ocean currents: red- warm, and blue- cold]. (B) Geomorphological map of the Porma valley showing the sampling site locations. The [10]Be CRE dataset includes a new set of 20 boulders sampled from lateral moraines in the Porma, Silván and Respina valleys; and two previous sets of boulders sampled from moraine, erratics and rock glacier boulders in the Porma (27 samples; Rodríguez-Rodríguez et al., 2016), and and Monasterio valleys (19 samples; Rodríguez-Rodríguez et al., 2017) [the acronym of the landform name is given in capital letters; information on boulder type is given by the following abbreviations: m-moraine boulder; e-glacial erratic boulder; rg- rock glacier boulder]. Black stars indicate the location of the new sediment cores and samples taken for OSL and radiocarbon dating; while grey stars indicate cores and OSL samples previously published in the Brañagallones and Tarna sites (Jiménez-Sánchez and Farias, 2002; Jiménez-Sánchez et al., 2013) is also included.

2. Methods

The sampling campaigns were planned considering previous geomorphological map and glacier reconstructions in the Porma valley (Rodríguez-Rodríguez et al., 2015, Rodríguez-Rodríguez et al., 2016).

2.1. Cosmic Ray Exposure dating

Surficial samples were collected from a total of twenty boulders from lateral moraines in the different tributaries of the Porma valley for ^{10}Be CRE analysis (sites ROB, RES, RUN and SIL in Fig. 1; Table 1). Five boulders per moraine were sampled with a manual jackhammer. Selected samples correspond to massive sandstone boulders embedded firmly at the top of moraine ridges, which represent statistically the best candidates for CRE dating (Heyman et al., 2016). All samples correspond to quartzarenite sandstone boulders with an estimated rock density of 2.65 g cm^{-3}. This lithology is only present within the study area in the Cambro-Ordovician Barrios Formation (Barrois, 1882), allowing us to use the geological map of the area (available at http://info.igme.es/visorweb/; last access on May 2018) for tracking the distance from potential source areas with regards to possible inherited concentrations of cosmogenic ^{10}Be. Samples were treated at the *Laboratoire National des Nucléides Cosmogéniques (LN$_2$C)* at *Centre Européen de Recherche et d'Enseignement des Géosciences de L'Environnement* (CEREGE, France). Physical sample pre-treatment included sample grain size lowering by mechanical crushing and magnetic separation with a Franz. Chemical treatment included three leaching batches (2 days duration each) in hydrofluoric acid to isolate and ensure quartz purification (Kohl and Nishiizumi, 1992). An amount of 14–18 g of pure quartz was spiked with ~0.1 g of Beryllium standard solution and digested in hydrofluoric acid. The Beryllium standard is an in-house solution (3025 ± 9 ppm ^{9}Be) prepared from a phenakite crystal mined at great underground depth

(Merchel, 2008, Braucher et al., 2015). Beryllium extraction was done using column chromatography and precipitation by neutralization. Beryllium hydroxides were dried after rinsing with pH 8 MQ water in order to remove isobar boron, and finally oxidized at 800ºC to BeO in porcelain crucibles. The isotopic ratio $^{10}Be/^9Be$ of each sample was measured at the French 5 MV AMS facility ASTER (Aix-en-Provence) (Arnold et al., 2010, Klein et al., 2008). Data were calibrated against three targets of reference material SRM4325 using an assigned $^{10}Be/^9Be$ ratio of $(2.79 \pm 0.03) \times 10^{-11}$ (Nishiizumi et al., 2007) and a ^{10}Be half-life of $(1.36 \pm 0.07) \times 10^6$ (Korschinek et al., 2010, Chmeleff et al., 2010). Reported analytical uncertainty includes external uncertainty of 0.5%, which accounts for all effects contributing to ASTER's variability and is based on long-term standard measurements (Arnold et al., 2010); counting statistics uncertainty of ca. 3% (~1000 events) and chemical blank correction uncertainty. The isotopic ratios measured for each sample were converted to ^{10}Be concentration in the quartz sample (Balco, 2006) and used to calculate exposure ages with the online exposure age calculator formerly known as the CRONUS-Earth ^{10}Be exposure age calculator (Balco et al., 2008) using version 2.3 (released in June 2016) and considering the global production rate based on the primary calibration dataset in Borchers et al. (2016) and the Lm scaling scheme (Lal, 1991, Stone, 2000) (Table 1). A standard atmosphere was assumed, while topographic shielding was corrected using the Cronus-Earth Geometric shielding calculator version 1.1 and field readings of the horizon's inclination taken at each sample site (Balco et al., 2008). Moraine minimum exposure ages reported in Table 1 correspond to straight mean of the exposure ages obtained from multiple boulders collected from the same landform, not corrected for neither erosion nor vegetation cover. Similarly, snow shielding corrections were not applied because the historical record of snowpack thickness measurements is too restricted in duration (c. 1991 to present) and spatial distribution

(just 5 control points, all placed along the Porma catchment divide) to ensure reliable corrections for the entire Last Glacial Cycle (Schildgen et al., 2005). Moreover, recent long-term neutron monitoring have shown that snow cover attenuates fast neutrons (0.1–10MeV) much more strongly than predictions based on conventional mass-shielding (Zweck et al., 2013), being necessary to develop further studies to validate the extrapolation of this results to spallogenic neutrons with higher energies (e.g. >50 MeV) like those responsible for ^{10}Be production (Delunel et al., 2014). Thus, the ages reported in this work must be regarded as minimum exposure ages. The ±1σ analytical uncertainty corresponds to the standard deviation of the mean exposure age when the standard deviation of the age values is greater than the averaged internal uncertainties. Otherwise, the standard deviation of the weighted mean is provided. Errors reported in brackets include uncertainty associated to the production rate.

2.*2. Radiocarbon dating*

Radiocarbon dating was applied to sediments deposited in ponds and peat bogs located outside lateral moraines or in glacially over-deepened hollows (Fig. 1). Eight sediment cores were drilled with a manual sampler manufactured by Eijelkamp®. Pond sequences and peat bogs formed outside lateral moraines (referred as ice dammed or kame terrace deposits) may have been deposited since the glacier advance responsible for the moraine deposition due to the impoundment effect on lateral tributaries, while ponds and peat bogs deposited in glacially over-deepened hollows most likely developed after glacier retreat. Once in the laboratory, each sediment core was split in half to describe the sedimentary sequence and take samples for radiocarbon dating. Ten terrestrial plant macro remains samples were taken from discrete organic-rich levels using laboratory pincers. Additionally, six bulk sediment samples were collected from some inorganic units. A slice ~0.5 cm thick of clay material was

Table 1

Minimum surface exposure ages reported for lateral moraines sampled in the Porma valley.

Sample ID	Lat (DD)[a]	Long (DD)[a]	Elevation (m)	Height (m)	Thickness (cm)	Shielding factor	Quartz (g)	Be carrier (mg)	[^{10}Be] (10^4 at g^{-1})[b]	^{10}Be CRE age (ka) [c] (3.97 ± 0.14 atoms g^{-1}a^{-1})
Runción lateral moraine										**20.2 ± 0.5 (0.9)[d]**
RUN-01	43.0368	-5.2835	1328	2.1	3.4	0.9975	14.5852	0.1025	24.574 ± 0.780	21.3 ± 0.7
RUN-02	43.0364	-5.2832	1331	1.4	2.3	0.9975	14.2067	0.1028	24.519 ± 0.795	21.1 ± 0.7
RUN-03	43.0357	-5.2825	1307	1.0	2.5	0.9978	14.7240	0.1014	22.965 ± 0.906	20.1 ± 0.8
RUN-04	43.0347	-5.2814	1278	4.6	2.5	0.9976	14.2754	0.1017	22.481 ± 1.073	20.2 ± 1.0
RUN-05	43.0338	-5.2807	1277	2.9	2.0	0.9980	15.0259	0.1027	20.414 ± 0.787	18.3 ± 0.7
Robledo lateral moraine										**21.0 ± 0.3 (0.8)[d]**
ROB-02	43.0233	-5.3224	1415	2.5	2.8	0.9982	14.6866	0.1024	24.313 ± 0.771	19.7 ± 0.6
ROB-03	43.0218	-5.3196	1390	1.5	1.8	0.9983	14.2943	0.1024	28.982 ± 0.922	23.6 ± 0.7
ROB-04	43.0218	-5.3196	1390	1.3	4.6	0.9983	14.1238	0.1023	42.908 ± 1.347	35.2 ± 1.1*
ROB-05	43.0218	-5.3196	1390	1.9	2.0	0.9983	14.9241	0.1018	28.238 ± 0.899	23.0 ± 0.7
ROB-06	43.0218	-5.3196	1390	1.4	4.0	0.9983	17.6897	0.1021	21.415 ± 0.729	17.9 ± 0.6
Respina lateral moraine										**27.1 ± 4.2 (4.3) [d]**
RES-01	43.0234	-5.3701	1631	1.1	2.0	0.9955	14.6739	0.1033	54.341 ± 1.704	36.4 ± 1.2
RES-02	43.0233	-5.3696	1644	1.2	3.0	0.9955	14.6324	0.1022	44.374 ± 1.471	29.9 ± 1.0
RES-03	43.0233	-5.3698	1644	0.9	3.3	0.9851	14.4383	0.1026	37.520 ± 1.329	25.8 ± 0.9
RES-04	43.0233	-5.3698	1644	0.9	1.7	0.9955	14.7452	0.1024	152.789 ± 4.762	101.7 ± 3.4*
RES-05	43.0231	-5.3696	1647	0.4	2.6	0.9955	14.5469	0.1022	23.721 ± 0.777	16.2 ± 0.5
Silván recessional moraine										**–**
SIL-01	43.0253	-5.3025	1256	0.6	1.6	0.9906	14.3810	0.1009	52.142 ± 1.632	46.3 ± 1.5
SIL-02	43.0251	-5.3027	1254	0.9	2.5	0.9442	14.4077	0.1031	53.506 ± 2.222	50.4 ± 2.2
SIL-03	43.0245	-5.3020	1262	0.8	2.0	0.9906	13.0997	0.1020	12.684 ± 0.591	11.6 ± 0.5
SIL-04	43.0246	-5.3020	1261	0.3	1.7	0.9906	14.8372	0.1028	15.040 ± 0.625	13.8 ± 0.6
SIL-05	43.0232	-5.3013	1263	-	2.5	0.9943	13.6479	0.1035	12.512 ± 0.720	11.5 ± 0.7

[a] Geographic coordinates are referred to WGS84 datum.

[b] Samples measured at the French AMS national facility ASTER (Aix-en-Provence, France).

[c] CRE ages calculated with the latest version of the online exposure age calculator formerly known as the CRONUS-Earth online exposure age calculator v2.3 (http://hess.ess.washington.edu/math/; November 2016; Balco et al., 2008) considering the default primary calibration dataset of Borchers et al. (2016) and the Lm scaling scheme. No snow and no erosion corrections were applied.

[d] Mean CRE age and analytical uncertainty, expressed as the standard deviation of the mean exposure age when the standard deviation is greater than the averaged internal uncertainties, otherwise, the standard deviation of the weighted mean is provided. Errors in brackets include production rate uncertainty (3.5%).

*Outlier boulder ages (see text for details).

taken in each case. Basal ages provide a minimum reference age for the start of the

sedimentation and thus for either the glacier advance episode responsible for lateral moraine

buildup or the glacier retreat episode that exposed a glacial hollow. All samples were

analyzed by the AMS radiocarbon technique in two commercial laboratories. Nine

radiocarbon samples were analyzed at Poznan Radiocarbon Laboratory (Poland) and seven

samples at Direct AMS laboratory (Seattle) (Table 2). Age results were calibrated with the

Radiocarbon Calibration Program Calib Rev 7.0.2 (Stuiver and Reimer, 1993) against the

IntCal13 curve (Reimer et al., 2013).

Table 2
Radiocarbon results obtained for samples taken from sediment cores drilled in key sites of the Porma valley closely related to past glacier environment. Radiocarbon ages calibrated with Calib Rev 7.0.2 program (Stuiver and Reimer, 1993) against the IntCal13 curve (Reimer et al., 2013).

Core ID	Depth (m)	Laboratory reference	Dated material	C-14 age (years BP)	Calendar age (2σ) (years BP)
Fonfría-01	1.73	Poz-76440	9 g wood	7000 ± 50	7712 – 7938
Fonfría-01	1.78	Poz-76441	3 g plant remains	6970 ± 50	7689 – 7876
Fonfría-01	4.02	Poz-76442	8 g plant remains	10450 ± 60	12104 – 12554
Fonfría-01	5.30	Poz-76443	4 g plant remains	9520 ± 60	10653 – 11099
Isidro-02	2.53	Poz-76447	13 g bulk sediment	33000 ± 500	36014 – 38473
Isidro-02	5.78	Poz-76448	12 g bulk sediment	40500 ± 1500	41842 – 46746
Silván-02	1.14	Poz-76450	15 g bulk sediment	6790 ± 50	7569 – 7709
Silván-02	1.94	Poz-76451	8 g bulk sediment	6950 ± 50	7679 –7869
Toneo-01	1.44	Poz-76452	12 g bulk sediment	14450 ± 70	17404 – 17870
Soportales-03	1.40	DAMS012594	24 g wood	5340 ± 33	6000 – 6211
Soportales-03	1.90	DAMS012595	13 g wood	7838 ± 39	8542 – 8729
Soportales-03	2.40	DAMS012596	38 g wood	8201 ± 36	9030 – 9272
Soportales-03	3.65	DAMS012597	7g wood	7686 ± 35	8411 – 8543
Soportales-03	4.20	DAMS012598	3 g wood	8158 ±34	9011 – 9143
Soportales-03	6.12	DAMS012599	1 g wood	8200 ± 38	9029 – 9274
Soportales-03	7.63	DAMS012600	8 g bulk sediment	27532 ± 122	31114 – 31531

14 *2.3. Optically Stimulated Luminescence dating*

15 The OSL technique was used to date sandy deposits from glacially-related sedimentary

16 basins and lateral moraines. A total of seven samples were taken (Table 3): (i) four samples

17 correspond to lacustrine sequences deposited in close relationship with lateral moraines,

18 either between moraine ridges (Tronisco site) or behind them (Guarilla site); (ii) two samples

19 correspond to lacustrine or alluvial sedimentary sequences infilling glacial hollows (Fonfría

20 and Remelende sites); and (iii) one sample (Runción site) is from a lateral moraine which

21 was also analyzed for [10]Be CRE dating. Samples were taken using conventional techniques

22 for poorly lithified sediments. Opaque plastic tubes were used to collect the samples and then

23 protected from light with the aid of plastic bags, tape and aluminum foil. Samples were

24 processed in the luminescence dating laboratory of *Instituto Universitario de Xeoloxía Isidro*

25 *Parga Pondal* at *Universidade da Coruña* (Spain). Sandy material of the tube ends (initial

26 ~5 cm) was discarded from the OSL analysis. Samples were dried at 45ºC and sieved to

27 collect the 180–250 μm grain size fraction, which was treated with hydrochloric acid to

28 remove carbonate and organic material. Both quartz and k-feldspar fractions were

29 independently leached with hydrofluoric acid. Quartz purity was ensured through Infrared

30 Stimulated Luminescence (IRSL) analysis of sample aliquots, obtaining negative signals in

31 all cases. The Equivalent Dose (ED) was measured using the Single Aliquot Regeneration

32 (SAR) protocol (Murray and Wintle, 2000), including a final recovery test. Measures were

33 performed in an automated RISØ TL/OSL-DA-15 reader equipped with a photomultiplier

34 EMI 9635 QA and an inner source of $^{90}Sr/^{90}Y$ that provides a dose of 0.120 ± 0.003 Gy/s.

35 Dose Rates (DR) were determined measuring the activity of ^{40}K, ^{238}U, ^{226}Ra and ^{232}Th in a

36 high-resolution Canberra spectroscopy at the radioactive laboratory at *Universidad de Sevilla*

37 (Spain). Results were used to determine the DR considering the conversion factors of Guerin

38 et al. (2011), while the cosmic dose was determined following Prescott and Hutton (1994).

39 The water content was measured in all samples and an average value was considered to

40 account for its effect over resultant DR. Table 3 compiles the OSL results, including the

41 number of aliquots measured and the over dispersion of the average in the distributions of

42 sample aliquots. The over dispersion shows the possible effect of sedimentation / transport

43 processes in the measured grains, which generally fits to a normal distribution (Galbraith et

44 al., 1999). In general, over dispersion values higher than 30% are related to these processes,

45 but also can result from low radiation rates. The Central Age Model was applied to estimate

46 sample ages (Galbraith et al., 1999). Samples Gua-02-1 and Gua-02-2 show over dispersions

47 above and below than 30% but provide the same burial age using this model. The OSL signal

48 of sample Fonf-01 was in saturated values, so a minimum age estimate is provided following

49 Wintle and Murray (2006).

50 **Table 3**
51 Optically Stimulated Luminescence results obtained for samples taken in the Porma valley (DR- dose rate;
52 ED- equivalent dose).

Sample ID	Depth (m)	Elev. (m)	Hum. (%)	DR (Gy/ka)	ED (Gy)	N	Overdisp. (%)	Age (ka)
Fonf-01	6.00	1600	20 ± 4	0.59 ± 0.07	< 96	10	-	< 164[a]
Gua-02-1	1.00	1350	20 ± 4	0.78 ± 0.08	25.5 ± 0.9	44	28.0 ± 5.8	32.5 ± 3.9
Gua-02-2	1.40	1350	17 ± 3	0.68 ± 0.06	19.2 ± 1.6	42	38.2 ± 6.9	27.9 ± 3.4
Tro-02-1	0.50	1500	29 ± 6	1.85 ± 0.22	9.4 ± 0.8	45	48.6 ± 6.1	5.0 ± 0.7
Runc-01	0.50	1340	20 ± 4	0.88 ± 0.13	29.4 ± 2.0	38	29.6 ± 5.7	33.3 ± 5.4
REM-02[b]	1.26	1640	10 ± 3	0.78 ± 0.09	20.6 ± 1.9	30	37.3 ± 8.5	26.5 ± 4.0
REM-02[c]	1.26	1640	16 ± 4	0.77 ± 0.09	21.0 ± 2.0	31	34.4 ± 8.4	27.0 ± 4.1

53 [a] The OSL signal obtained from quartz was saturated most probably due to insufficient bleaching prior to the final burial
54 event dated. The age provided is a minimum estimate based on Wintle and Murray (2006).
55 [b] Aliquot of REM-02 sample that corresponds to the 180-250 μm grain fraction.
56 [c] Aliquot of REM-02 sample that corresponds to the 250-300 μm grain fraction.

57 **3. Results**

58 Four lateral moraines preserved along the Porma, Isoba, Respina and Silván valleys were

59 sampled for cosmic ray exposure dating (Table 1) and resultant ages have been analyzed

60 against [14]C (Table 2) and OSL (Table 3) results derived from lacustrine sediments closely

61 related to glacier dynamics and moraine deposition. Results are summarized by sampling

62 areas.

63 **3.1. The Porma valley and the Señales Pass**

64 The Porma valley (~12 km long; up to 1.5 km wide) shows outstanding examples of lateral

65 moraines, particularly well-preserved are those located in the vicinity of the Cofiñal village

66 and at the confluence with the Tronisco tributary valley. The Runción moraine is a 1.2 km-

67 long lateral moraine preserved in the western slope of the Porma valley, hanging ~200 m

68 above the valley floor. The ^{10}Be CRE dating of five boulders from this moraine yielded a

69 mean minimum abandonment age of 20.2 ± 0.5 (0.9) ka, whereas an OSL sample from the

70 sandy till matrix of the same moraine (Runc-01) provide a minimum burial age of 33.3 ± 5.4

71 ka for the time of moraine deposition (Fig. 2). A sediment core was drilled in the Guarilla

72 kame terrace (ca. 1350 m a.s.l.) deposited behind the Runción lateral moraine and named

73 Guarilla-02. It is made up by alternations of clay, silt and sandy sediments interpreted as

74 lacustrine sedimentation with episodic alluvial inputs from a lateral short tributary (~1.1 km

75 long). Two OSL analysis of the sandy sediment found at 1.0 and 1.4 m depth provide burial

76 ages of 27.9 ± 3.4 and 32.5± 3.9 ka respectively (Table 3), which represent minimum ages

77 for the onset of alluvial sedimentation due to the impoundment of the lateral tributary valley

78 caused by the presence of the Runción lateral moraine.
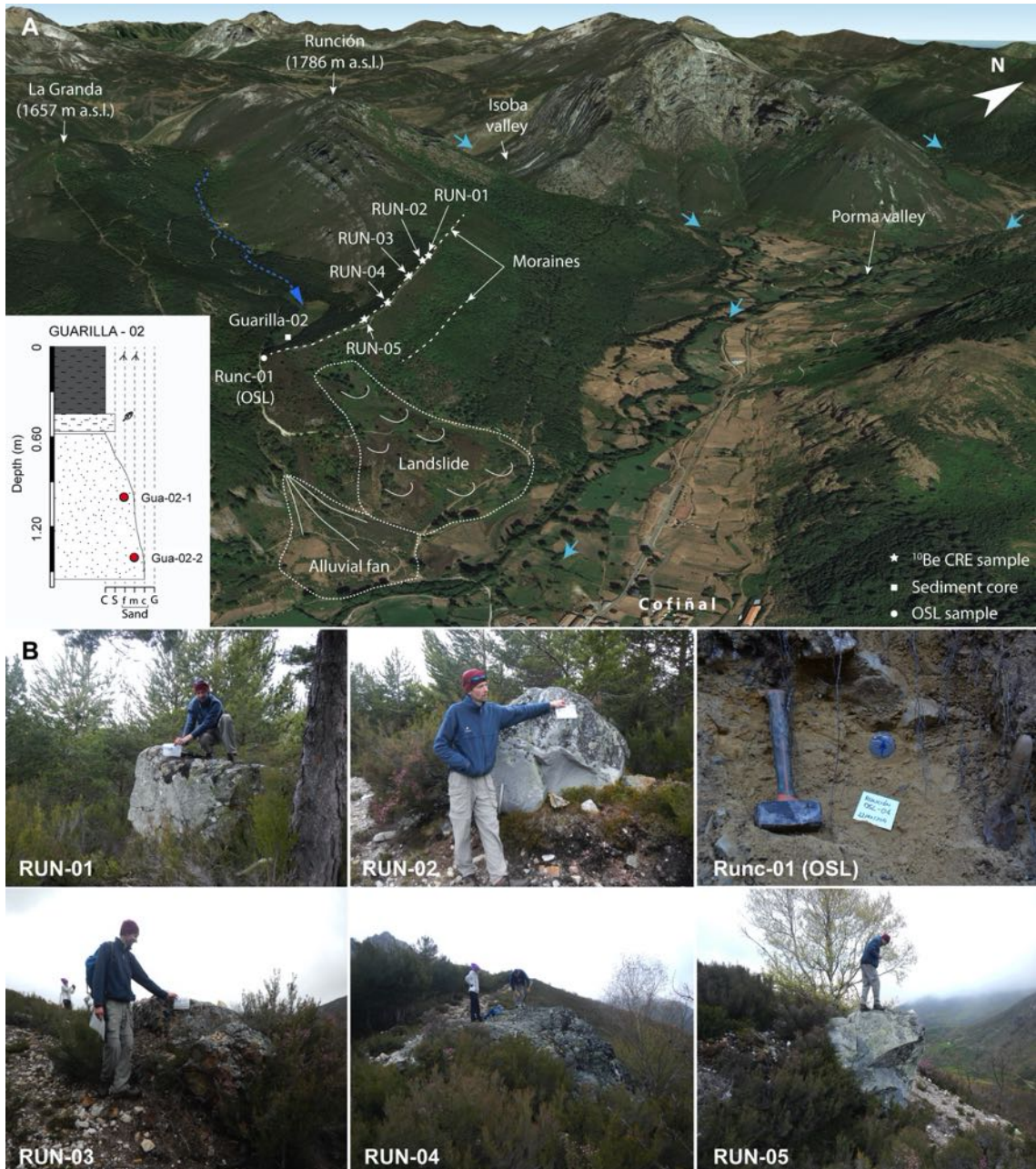
Figure 2.- (A) Google Earth image showing the location of the Runción lateral moraine and the Guarilla kame terrace in the Porma valley, which were dated through a combination of [10]Be CRE and OSL dating (small blue arrows indicate former ice flow direction). Particle size in the stratigraphic section of the Guarilla-02 core is provided according to the Wentworth scale [C- clay; S- silt; Sf- fine sand; Sm- medium sand; Sc- coarse sand; G- gravel]. (B) Detailed pictures of sampled boulders in the Runción moraine and the OSL sample Runc-01 taken from the till matrix in an exposed section of the same moraine (about one-meter depth below surface).

About 2 km up-valley from Cofiñal, five lateral moraines are preserved at different heights across the Tronisco tributary valley, the outermost towering up to 200 m above the floor of the Porma valley. Due to the scarcity of adequate boulders for [10]Be CRE dating, only a

15

89 sediment core named Tronisco-02 was drilled in a lacustrine deposit preserved between the

90 two outermost moraine ridges (Fig. 3A). This core reached a depth of 0.8 m, showing a lower

91 unit (~25 cm) made up by matrix-supported angular sandstone cobbles embedded in a sandy-

92 clay matrix interpreted as till sediments; and an upper unit composed by fine sand and silt

93 sediments (~55 cm) interpreted as the result of illuviation from the adjacent moraines. The

94 OSL sample Tro-01 was taken in the Tronisco-02 core at a depth of 0.5 m and yielded a

95 burial age of 5.0 ± 0.7 ka for the alluvial inter-moraine sequence.

96 A third site was analyzed in the Zampuerna tributary valley close to the Remelende peak

97 (1888 m a.s.l.; Fig. 3B), which is located 0.5 km north from Las Señales Pass (1625 m a.s.l.)

98 and ~2.4 km west from the Tarna Pass (1492 m a.s.l.). Alluvial sand sediments nested within

99 two recessional moraines at ~1640 m a.s.l. were sampled for OSL analysis (sample REM-

100 02). The source area of alluvial sand sediments is located at a distance of 0.5–1 km. The OSL

101 analysis was performed on two different grain size fractions of the REM-02 sample (180-250

102 μm and 250–300 μm), resulting in ages of 26.5 ± 4.0 and 27.0 ± 4.1 ka, which ideally

103 represent a minimum time reference for the onset of alluvial sedimentations at this setting.

104 **3.2. The Isoba valley and the San Isidro Pass**

105 The Isoba valley is an 8.8 km-long valley that extents from the San Isidro Pass (1520 m a.s.l.)

106 to its confluence with the Porma valley. Previous [10]Be CRE chronologies based on analysis

107 of rock glacier boulders and glacial erratics resting on the ice-molded surface of Loma

108 Fonfría were complemented with new radiocarbon and OSL analyses from three glacially-

109 related sedimentary sequences (Figs. 4 and 5). Particularly, sediment cores correspond to: (i)

110 the Isoba valley bottom located between the San Isidro urbanization and the San Isidro Pass

111 (Isidro-02); (ii) the Fonfría peat bog (Fonfria-01) located in the Loma Fonfría surface; and

112 (iii) the Toneo kame terrace (Toneo-01) located East from the San Isidro valley.

113
114 **Figure 3**.- (A) Google Earth image showing the location of lateral moraines preserved in Arroyo de Tronisco
115 and location of the sediment core Tronisco-02 (where the OSL sample Tro-02-1 was taken) between the two
116 outermost lateral moraines. (B) Panoramic Google Earth view of the Señales and Tarna mountain passes. The
117 location of the Tarna core, previously dated with a combination of radiocarbon and OSL techniques, is also
118 provided (Jiménez-Sánchez and Farias, 2002; Jiménez-Sánchez et al. 2013). (C) An OSL sample was taken in
119 alluvial sediments nested by recessional moraines in the vicinity of the Señales Pass. Small blue arrows
120 represent former ice flow directions.
121
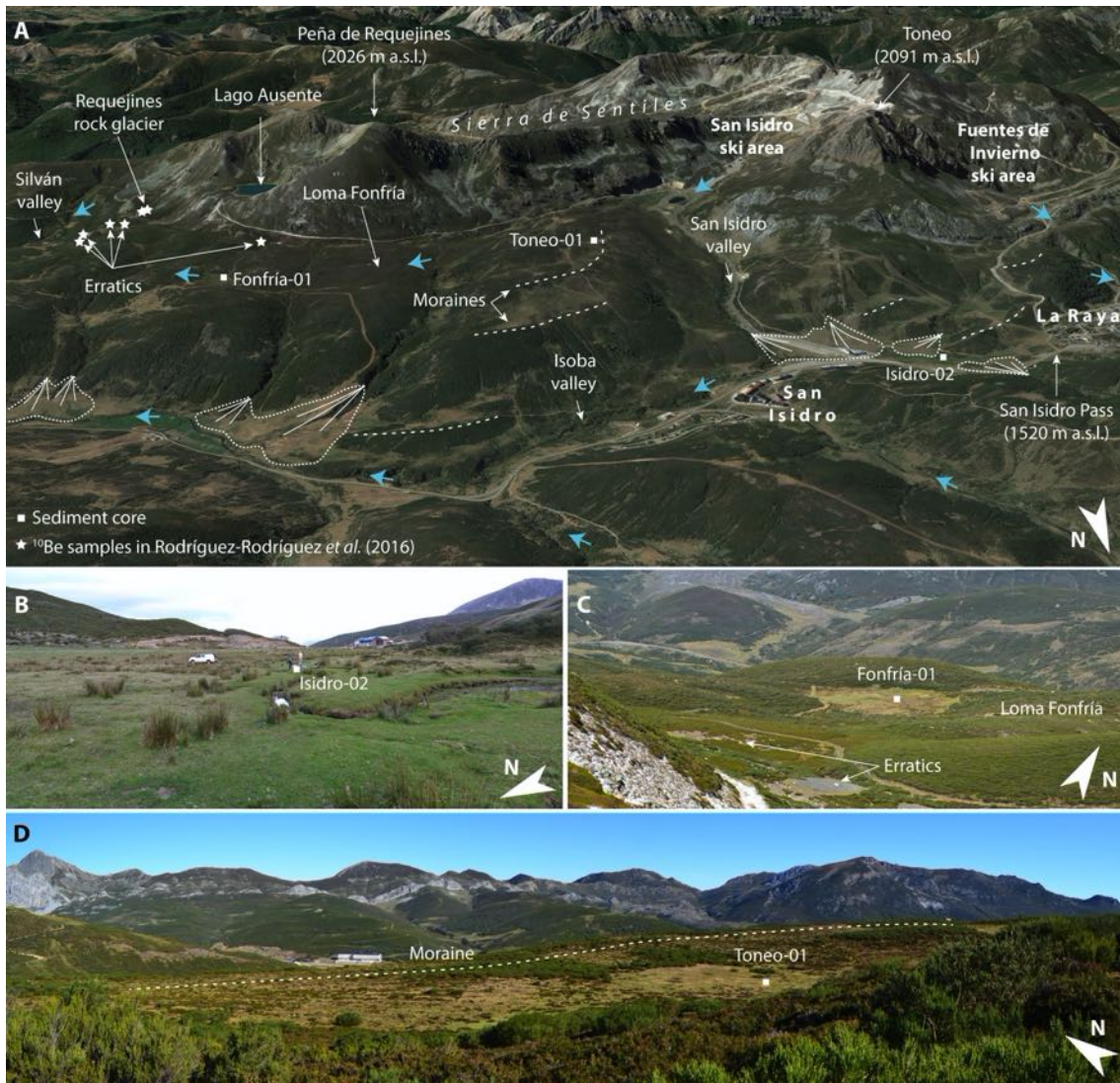
Figure 4.- (A) Google Earth image of the Isoba and San Isidro valleys and former ice flow directions (small blue arrows). The locations of the following sediment cores studied are provided: (B) valley bottom infill sequences (Isidro-02); (C) infill sequences deposited in glacially over-deepened depressions (Fonfría-01); and (D) kame terraces deposited outside lateral moraines (Toneo-01). The locations of previous [10]Be CRE dated glacial erratics and rock glacier boulders are also indicated (Rodríguez-Rodríguez et al., 2016).

The Isidro-02 core was retrieved from a valley bottom infill sequence deposited in the Isoba glacial valley close to the confluence with the San Isidro valley and located about 450 meters east of the San Isidro Pass (Fig. 4B). This sequence is at least 6.2 m thick, composed of decimeter-sized intervals of grey gravel and sand units, inter-bedded with grey silt and clay intervals arranged as normal grading sequences interpreted as alluvial sedimentation related to inputs from nearby tributary valleys. Gravel sediments are mostly made up by bedrock

134   shale and sandstone fragments up to 2-3 cm in diameter. A thick unit of dark grey clay is

135   preserved at depth between 4.50 and 5.85 m and is interpreted as decantation of fine

136   sediments in a quiet lacustrine environment. A second yellowish to brownish colored clay-

137   silt laminated unit is preserved at depth between 1.80 and 2.55 m and may correspond to

138   glacial varve sediments. Two radiocarbon bulk sediment samples were analyzed at the base

139   of the two clay units. The sample taken at the base of the deepest homogeneous clay unit

140   yields an age of 41.8–46.7 cal ka BP, while the bulk sediment sample at the base of the varve

141   interval yields an age of 36.0–38.5 cal ka BP.

142   The Fonfría-01 core corresponds to a peat bog sequence deposited in a glacially over-

143   deepened depression that was excavated in the Loma Fonfría ice-molded surface (~1520–

144   1670 m asl; ~3.3 km SE of the San Isidro Pass Fig. 4C). The Fonfría-01 core reached a drilling

145   depth of 6.3 m, showing a sequence constituted of 0.7 m-thick lower unit of alluvial quartz-

146   rich sands overlaid by alternations of lacustrine clay-silt sediments and peat bog material.

147   The source area of the basal sandy unit is located just 300 to 600 m south from the Fonfría

148   sequence, in the quarztarenite sandstone that outcrops along Sierra de Sentiles. Given the

149   absence of alluvial sands in the upper part of the core and the dominance of muddy and peat

150   bog intervals, a glacio-fluvial origin is assumed for the basal sandy unit, which was probably

151   deposited when glaciers were retreating from the Loma Fonfría surface. In fact, the OSL

152   sample taken at 6 m depth provided a saturated OSL signal for quartz, most likely due to

153   insufficient bleaching prior to burial. Four radiocarbon samples from the upper peat bog

154   intervals were analyzed for radiocarbon, and the oldest minimum depositional age for the

155   lacustrine sedimentation is 12.1–12.6 cal ka BP. However, this result does not correspond to

156   the deepest sample in this core.
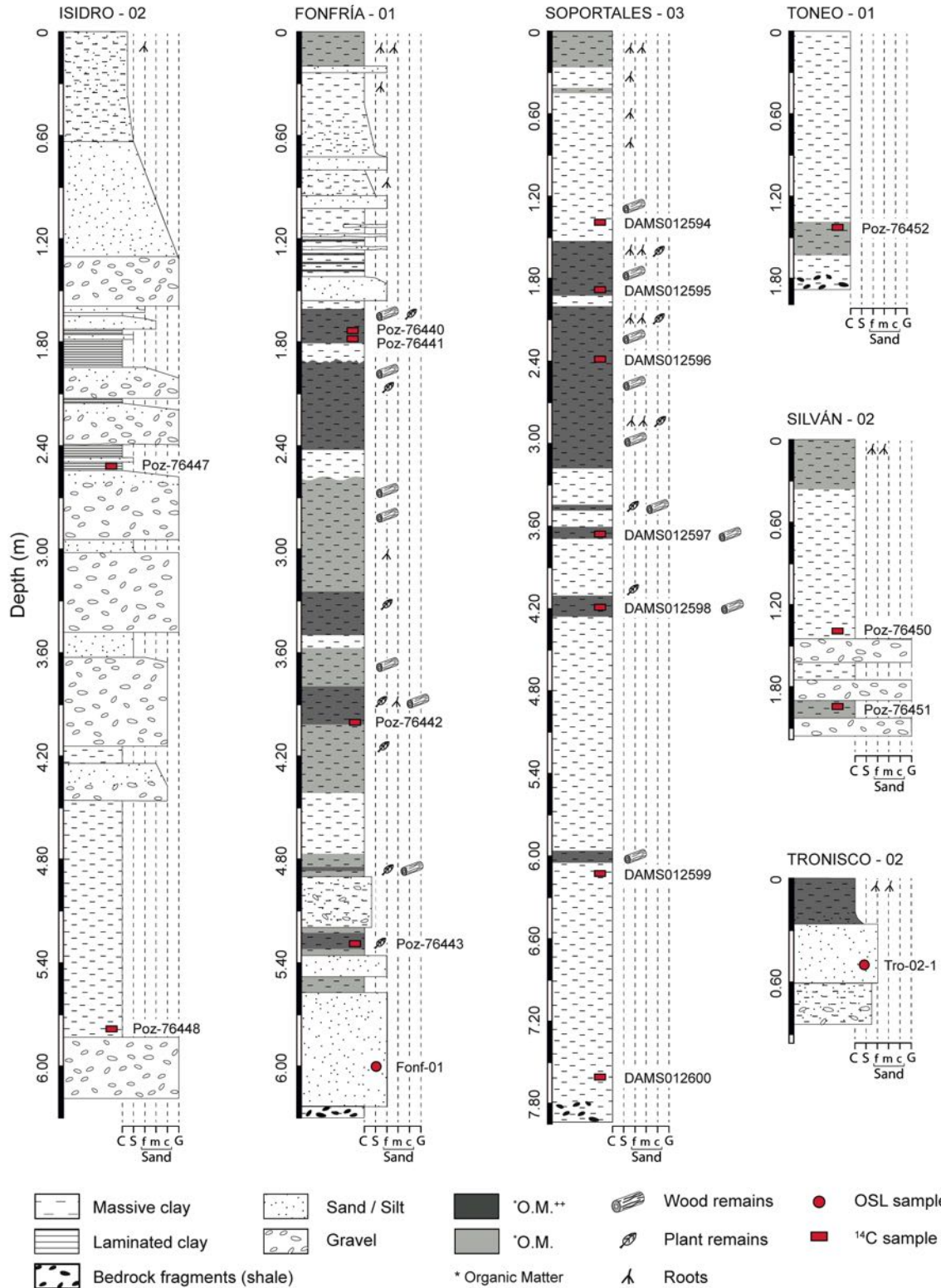
Figure 5.- Sedimentary sequences of the Isidro-02, Fonfría-01, Soportales-01, Toneo-01 Silván-02 and Tronisco-02 cores [particle size according to the Wentworth scale: C- clay; S- silt; Sf- fine sand; Sm- medium sand; Sc- coarse sand; G- gravel]. The position of radiocarbon and OSL samples in the sedimentary sequences is indicated and results are provided in Tables 2 and 3. Core locations are shown in Figure 2.

162   Finally, the Toneo-01 core was drilled in a kame terrace deposited behind the lateral moraine

163   located along the eastern slope of the San Isidro valley (Fig. 4D). The sequence is at least 1.7

164   m thick and mostly comprises grey massive clay sediments. A bulk sediment sample taken

165   close to the base of the Toneo-01 core gives a minimum radiocarbon age of 17.4–17.9 cal ka

166   BP.

167   **3.3. The Silván and Respina valleys**

168   The Silván valley is the main tributary of the Porma valley in the study area (Fig. 6). This

169   9.8 km-long glacial valley extends from the vicinity of Lago Ausente to Puebla de Lillo

170   village. Well-preserved lateral moraines on both valley sides can be observed continuously

171   over 2 to 3.6 km. The lateral moraine preserved along the western side of the Silván valley

172   is merged with the lateral moraine that runs along the northern slope of the Respina valley

173   (also known as Iyarga valley). The Respina valley is a 7.7 km-long glacial valley that starts

174   at the southern side of Sierra de Sentiles. Former glaciers that flowed along the Silván and

175   Respina valleys joined at the Soportales area, where multiple medial moraines were deposited

176   and preserved. The Soportales-03 core corresponds to a 7.9 m thick lacustrine sequence

177   deposited between moraine ridges preserved at the former water divide between the Rebueno

178   and Celorno valleys. The core is located at 1270 m a.s.l., ~58–74 m above the modern

179   Celorno river. The sequence alternates lacustrine grey clay and dark-brown peat bog material

180   intervals with multiple plant macro remains such as wood fragments, pine corns, and

181   hazelnuts. The lowest unit corresponds to clay and angular shale fragments interpreted as

182   weathered bedrock. Seven radiocarbon ages were obtained from the Soportales-03 core, six

183   correspond to wooden fragments, whereas the deepest sample corresponds to bulk sediment.

184   Radiocarbon ages obtained from woody fragments sampled at depths between 1.42 and 6 m

185 yield ages in the range 6.0–9.3 cal ka BP. However, the lowest bulk sediment sample taken

186 at 7.6 m depth yields an age of 31.1–31.5 cal ka BP.

187
188 **Figure 6.**- (A) Google Earth view of the Silván, Respina and Rebueno-Celorno tributary valleys in the Porma
189 basin, showing former ice flow directions (blue arrows) during the local Glacial Maximum and the location of
190 the Robledo and Respina moraines sampled for [10]Be CRE dating (detailed pictures of the sampled boulders are
191 also provided). The location of the sediment cores Silván-02 and Soportales-03 drilled in lacustrine infill
192 deposited in glacially over-deepened depressions and between lateral moraines is also indicated. (B) Panoramic
193 view of the Respina moraine and detailed pictures of the sampled boulders. The ridge of a recessional moraine
194 placed inside the Respina moraine is also indicated but was not sampled for CRE dating.

22

195   Two lateral moraines were sampled for [10]Be CRE dating in the Respina valley. These were

196   informally named Robledo and Respina moraines in this work (Fig. 6). The Robledo lateral

197   moraine is a 2.2 km long lateral moraine preserved along the northern slope of the Respina

198   valley, hanging ~160 m above the valley floor. A mean minimum exposure age of 21.0 ± 0.3

199   (0.8) ka is reported based on [10]Be CRE analysis of four boulders. Boulder ROB-04 was

200   excluded from the moraine mean exposure age because it is more than two standard

201   deviations older than the other four boulders. The Respina lateral moraine is 380 m long, ~37

202   m high, and is perched 208 m above the Respina valley floor close to the old Respina talc

203   mine. A minimum [10]Be CRE age of 27.1 ± 4.2 (4.3) ka is estimated for the Respina lateral

204   moraine based on ages from four boulders. The age of boulder RES-04 was excluded from

205   the moraine mean exposure age because it is more than two standard deviations older than

206   the mean exposure age of the other four boulders.

207   In the Silván valley, a 430 m-long recessional moraine draping a bedrock step ~70 m-high

208   above the valley floor was sampled for [10]Be CRE dating (Fig. 7). The results clearly show

209   two distinct groups of boulder exposure ages (Table 1). Two boulders provide ages of 46.3

210   $\pm$ 1.5 ka (SIL-01) and 50.4 ± 2.2 ka (SIL-02), and are older than expected according to the

211   relative age sequence and comparable to ages previously reported for the Redipollos erratics

212   4 km down-valley (Rodríguez-Rodríguez et al., 2016). The remaining three boulders yielded

213   results in the range 13.8 to 11.5 ka (SIL-03 to 05) which are considerably younger than

214   expected according to previous ages reported for glacial erratics resting on the Fonfría surface

215   (17.7 $\pm$ 0.4 ka) and the Requejines rock glacier (15.7 $\pm$ 0.3 ka) (Rodríguez-Rodríguez et al.,

216   2016). Thus, it is not possible to calculate a mean CRE age representative for the time of

217   moraine abandonment. Considering the minimum exposure ages obtained from the Runción,

218   Robledo and Respina lateral moraines and the ages of glacial erratics lying on top of the

219 Loma Fonfría surface, the most probable abandonment age of the Silván moraine should lie

220 between 20 and 17.7 ka. An alternative interpretation is that instead of a recessional moraine,

221 the Silván ridge is not a recessional moraine but draping till partly preserved on a topographic

222 high that was overridden by glaciers during multiple glacial stages. Then, the inherited

223 boulders reflect a reference age for the glaciers overriding this site and flowing down to the

224 terminal zone.

225
226 **Figure 7.-** The Silván moraine (ca. 1263 m a.s.l.) is draping a bedrock step ~70 m-high above the Silván valley
227 floor. This site was exposed when the Silván outlet glacier had thinned about 60 m compared to the previous
228 glacial stage marked by the ROB lateral moraine, in the opposite hillslope.

229   Located on the distal side of the Silván moraine, a sediment core named Silván-02 (1.76 m

230   thick) was drilled in a glacially over-deepened hollow excavated in the Carboniferous shale

231   bedrock. The Silván-02 sequence is mostly composed of laminated clays of lacustrine origin

232   and coarser sediment intervals washed from the nearby SIL moraine (Fig. 5, Fig. 6A). Two

233   radiocarbon samples were analyzed, providing a minimum reference age of 7.7–7.9 cal ka

234   BP for the onset of lacustrine sedimentation at this site.

235   **4. Discussion**

236   The application of the three most frequently used dating techniques for studying glacial and

237   glacial-related deposits in a single study area offers a unique opportunity to: (i) analyze dating

238   results relying on different techniques; and (ii) improve the chronological framework of

239   Quaternary mountain glaciations in the Cantabrian Mountains, and (iii) identify potential

240   forcing involved in the glacial history of the studied area.

241   **4.1. Similarities and discrepancies between dating results relying on the different**

242   **techniques**

243   The new [10]Be CRE chronology presented in this work is generally time-consistent with

244   previous [10]Be CRE ages reported for the glacial sequence in the Porma valley (Rodríguez-

245   Rodríguez et al., 2016). The minimum abandonment ages obtained in the Runción (20.2 ±

246   0.9 ka), Robledo (21.0 ± 0.8 ka) and Respina (27.1 ± 4.3 ka) lateral moraines support our

247   previous hypothesis that glaciers were still filling the main valleys during MIS 2, flowing

248   down to an elevation of 1130 m a.s.l. Particularly, glacier tongues flowing along the Porma,

249   Silván and Respina valleys would have reached ice thickness values comparable to those

250   recorded during the previous Pleistocene glacial maximum, adding new till deposits to the

251   already existing lateral moraines. Only the Silván recessional moraine yielded an anomalous

252   mixture of boulder exposure ages that are either too old or too young compared to the

253   moraines and rock glacier sequence dated up and down-valley. According to previous

254   analyses of large global datasets, partial exposure due to post-depositional shielding occurs

255   more often than over-exposure with respect to the deposition time due to prior exposition

256   (Heyman et al., 2011). In the present study, boulder ages that are more than two standard

257   deviations older than the rest of the group mean age are considered too old and excluded

258   from the average moraine age calculation (time of moraine abandonment). They are probably

259   related to either insufficient erosion prior to exposure, e.g. the minimum travelling distance

260   estimated for these boulders varies between 2 and 0.1 km; or inherited nuclides from previous

261   episodes of exposure during glacier advance and retreat in the area, e.g. boulders RES-04,

262   SIL-01 and SIL-02 yield ages that are comparable to those previously found at the glacier

263   front area and attributed to past glacier advances during MIS 5d and MIS 3.

264   Radiocarbon dating in lacustrine environments may be affected by contamination related to:

265   (1) sediment reworking of old organic matter; (2) freshwater reservoir or hard-water effect

266   (lake freshwater contaminated by old carbon from bedrock can cause the aging of new

267   organic matter synthetized in the aquatic environment); and (3) inorganic carbon

268   contamination as fine-grained sediments derived from bedrock (Pallàs et al., 2006).

269   Radiocarbon samples were preferentially taken from terrestrial plant macro remains to

270   minimize the freshwater effect (Rixhon et al., 2017). Our results show that in general bulk

271   sediment samples provided results considerably older than those obtained from plant macro

272   remain samples. In multiple cases, these virtually old radiocarbon results do not conflict with

273   numerical ages obtained with [10]Be CRE and OSL techniques in adjacent settings, respecting

274   the relative age sequence. In contrast, the Isidro-02 sequence deposited as a valley bottom

275   infill at the confluence between the San Isidro and Isoba valleys, reveals two unexpectedly

276   old radiocarbon results, both derived from bulk sediment samples. They suggest that the

277   valley was ice free and was recording alluvial and lacustrine sedimentation since 41.8–46.7

278   cal ka BP, which is incompatible with chronological evidence based on both [10]Be CRE and

279   OSL. The age differences between plant-macro remain and bulk sediment samples are more

280   evident when we compare the sedimentation rate at the different sites (Fig. 8). Toneo-01 and

281   Isidro-02 (bulk sediment samples) suggest low and relatively uniform sedimentation rates,

282   whereas Fonfría-01, Soportales-03 and Silván-02 show higher sedimentation rates,

283   particularly during the Early Holocene. In the Soportales-03 core, the basal age based on bulk

284   sediment provides an age ~22 ka older than the numerical ages derived from plant macro

285   remain samples at lower depths. The fact that all bulk sediment samples display radiocarbon

286   ages that are too old strongly suggests a possible aging effect due to inorganic/mineral

287   ('fossil') carbon contamination similar to the one previously observed in multiple lacustrine

288   sequences in the Pyrenees (Pallàs et al., 2006). In addition, all potentially aged bulk sediment

289   samples correspond to lacustrine environments developed on top of Carboniferous bedrock,

290   consisting on shale and sandstone alternations that can sporadically present inter-bedded thin

291   coal layers. Radiocarbon analysis based on pollen concentrates could be the best alternative

292   to get reliable numerical results. Regarding age inversions in radiocarbon results, they were

293   mostly found in Soportales-03 core between 2 and 6 m depth and could be related to soil

294   carbon reservoir effect (Jull et al., 2013) or to duplicated material accidentally resampled

295   from the well walls during successive drilling maneuvers.
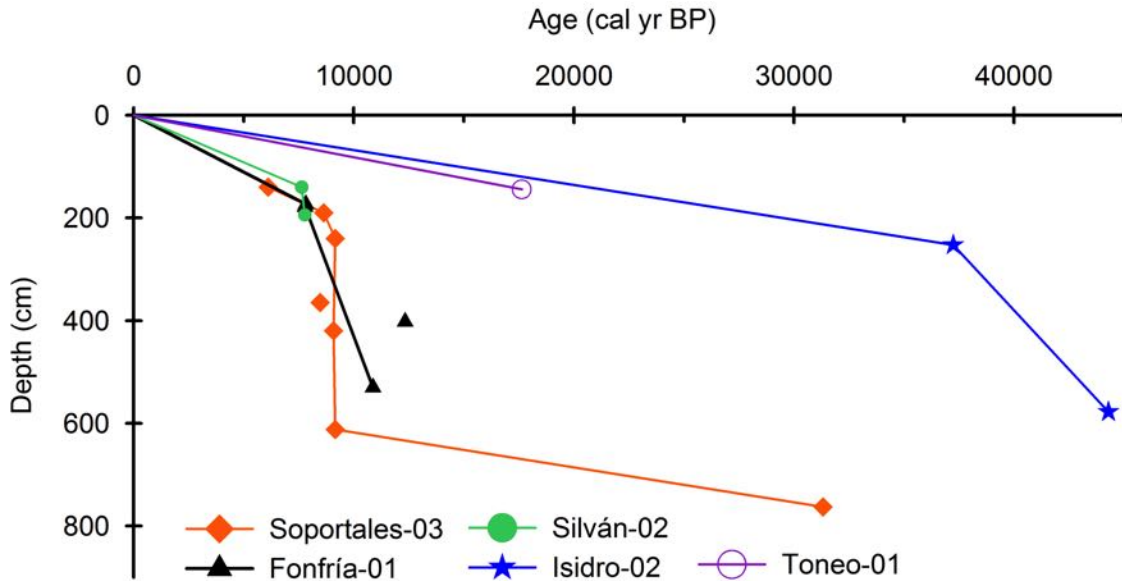
Figure 8.- Comparison between sedimentation rate trends observed in the different cores based on radiocarbon numerical ages. The sequences Silván-02, Fonfría-01 and Soportales-03 show similar tendency in sedimentation rate during the Holocene. In contrast, Toneo-01 and Isidro-02 (ages exclusively obtained on bulk sediment samples) suggest markedly lower sedimentation rates, probably because results are contaminated by dead carbon effect inherited from local bedrock. Isidro-02, Toneo-01 and Soportales-03 ponds developed on top of Carboniferous shale and sandstone with eventual coal intervals. Thus, inorganic 'fossil carbon' may have incorporated to these sequences as fine-grained particles. The same is observed for the basal age of the Soportales-03, also obtained from a bulk sediment sampled.

Regarding OSL results, insufficient light exposure prior to burial is the commonest source of biased results when this technique is applied to date glacial and glacio-fluvial sediments. In the case of glacio-fluvial materials, glacial meltwaters usually have large amounts of suspended sediments that can prevent light-rays to efficiently penetrate through the water column (Stockes, 1999, Klasen et al., 2007). Meanwhile, tills can potentially be transported within the glacier or close to its base (sub-glacially) without necessarily being exposed to light-rays prior to burial. In our case study, all samples gave poor luminescence intensities (highly insensitive to irradiation) and required a large amount of aliquots to get an age determination. The results obtained from the till samples of the Runción lateral moraine (33.3 ± 5.4 ka) and the Guarilla kame terrace deposited behind (27.9 ± 3.4 and 32.5 ± 3.9 ka) yield burial ages that are time-consistent with the [10]Be CRE chronology of the Runción moraine. Additionally, results are comparable to the previous OSL age of 24.0 ± 1.8 ka reported for

317 one of the outermost lateral moraine ridges that dammed the Brañagallones kame terrace

318 sequence in the north-facing Monasterio valley (Jiménez-Sánchez et al., 2013), which also

319 shows burial age few thousands of years older than the [10]Be CRE ages obtained for the

320 recessional moraine sequence preserved inwards (Rodríguez-Rodríguez et al., 2017). In

321 contrast, OSL burial ages obtained in an alluvial fan close to the Remelende peak (26.5 to 27

322 ka) suggest that some areas along the North-South divide of the Cantabrian Mountains may

323 have remained ice-free during the LGM. This is also supported by material dated in the Tarna

324 valley, where radiocarbon analysis at the base of the Tarna sequence (~600 m North from the

325 Tarna Pass) and OSL analysis of a post-glacial landslide deposit yielded results of 24.6 ± 0.4

326 cal ka BP and 23.0 ± 2.3 ka, respectively (Jiménez-Sánchez and Farias-Arquer, 2002,

327 Jiménez-Sánchez et al., 2013). However, both the Guarilla and Remelende sequences were

328 deposited by steep alluvial streams as short as ~1.1 km, so these sandy units were potentially

329 deposited by turbid water currents, an environment more prompt for insufficient bleaching

330 prior to burial (Rixhon et al., 2017). In the case of the basal sandy unit at the base of the

331 Fonfría sequence, the OSL saturated signal obtained for quartz confirms that this unit was

332 not fully bleached before burial. The absence of other sand intervals in the rest of the Fonfría

333 infill sequence could be consistent with a glacio-fluvial origin related to meltwaters sourced

334 from receding glaciers.

335 **4.2. The long-term evolution of glaciers in the central Cantabrian Mountains deduced**

336 **from the Porma and Monasterio datasets**

337 Together, the Porma and Monasterio sequences provide a complete picture of the Last

338 Glaciation in the central Cantabrian Mountains in northern Spain. Although the terminal

339 moraines are not preserved in the Porma catchment, the remaining glacial evidence suggests

340 that the first glacial stage (Stage I, Fig. 9) of the Last Glacial Cycle took place early (~ 110

341 ka) coevally with MIS 5d. Some boulders provide even oldest ages (~170–150 ka) that might

342 be inherited from a previous glaciation during MIS 6 (Rodríguez-Rodríguez et al., 2016). In

343 contrast, evidence of these old glacial advances has not been found in the northern slope yet,

344 probably because the topography is generally steeper and the valleys are narrower, conditions

345 that did not favor the preservation of glacial evidence.

346 The Porma glacier margins remained in positions close to the previous stage during MIS 3

347 and MIS 2 (~56–22 ka; Stages IIa to IIb), as indicate the presence of diachronous boulders

348 (like RES-04) in various lateral and medial moraines (e.g. RES, ROB and LIL moraines) that

349 suggest moraine build-up during several glacial stages or even during long-time periods. The

350 burial OSL ages obtained in the Runción lateral moraine (c. 33.3 ka) and the Guarilla kame

351 terrace (ca. 32.5 ka) also support continuous glacial occupation of the Porma catchment

352 during MIS 3 (Stage IIa) until the LGM culmination (Stage IIb). The radiocarbon basal age

353 of the Soportales-03 sequence (31.1–31.5 cal ka BP) is consistent with minimum deglaciation

354 ages obtained in the CEL erratic boulders and suggest glacier free conditions for the Celorno

355 valley by the time of the LGM culmination (Stage IIb; Fig. 9). In the northern slope of the

356 range, Stage IIb is recorded by the minimum radiocarbon age of ~33.5 cal ka BP obtained

357 close to the base of the Brañagallones kame terrace sequence, outside the outermost lateral

358 moraine (Jiménez-Sánchez and Farias-Arquer, 2002), while a burial OSL age of c. 24 ka

359 (Brañag-1) has been reported for an inner moraine ridge of the same complex (Jiménez-

360 Sánchez et al., 2013). Evidence for glacier oscillations through MIS 3 have been previously

361 reported to the East, in the glacio-lacustrine sequences of Comeya (~45 ka; Jiménez-Sánchez

362 et al., 2013), Belbín (~37.2 cal ka BP; Ruíz-Fernández et al., 2016) and Campo Mayor (~35.3

363 cal ka BP; Serrano et al., 2012) in Picos de Europa. Minimum radiocarbon ages reported for

364 Laguna del Castro (~44 cal ka BP) and Laguna del Miro (>35 cal ka BP) in Laciana (Jalut et

al., 2010) and the OSL age of supraglacial till sediments from Vega del Naranco terminal moraine at Fuentes Carrionas Massif (~36 ka; Serrano et al., 2013) are equally consistent with the glacial record documented here for the central Cantabrian Mountains.

The minimum exposure ages of the RUN and ROB lateral moraines suggest that the last deglaciation started at c. 21–20 ka in the central Cantabrian Mountains, consistently with the evolution of the Sanabria Lake record (Rodríguez-Rodríguez et al., 2014). The [10]Be CRE age dataset of the Monasterio valley indicates a consistent deglaciation sequence with recessional stages at minimum ages of c. 18.1 ka; 16.7 ka; and 14 ka (Rodríguez-Rodríguez et al., 2017). In the Porma valley, a population of erratic boulders resting on top of Loma Fonfría ice-molded surface suggest remarkable ice thinning of local glaciers by c. 17.7 ka (Rodríguez-Rodríguez et al., 2016) that are consistent with the new minimum radiocarbon ages reported in this work for the Fronfría-01 (12.1–12.6 cal ka BP) and Toneo-01 (17.4–17.7 cal ka BP) sequences (Fig.9). Regarding the timing of rock glacier activity (periglaciation), available [10]Be CRE chronologies for two rock glaciers suggest the stabilization of the foremost ridge during the time interval ~15.7–13 ka (Rodríguez-Rodríguez et al., 2017, Rodríguez-Rodríguez et al., 2016). The available deglaciation datasets show apparently longer time resilience of glaciers in the northern slope of the range compared to the southern slope, possibly favored by topo-climate conditions (although further studies are required to confirm this).
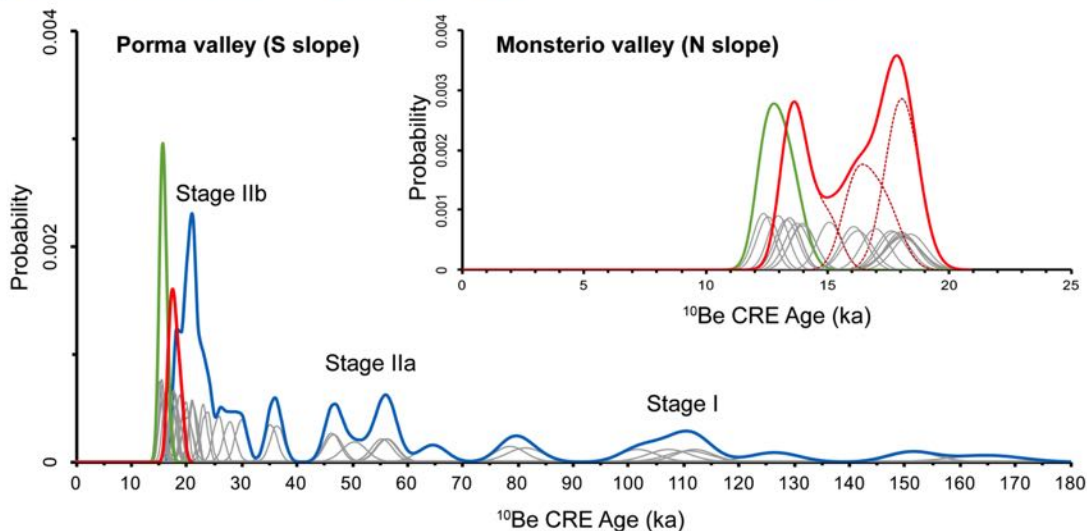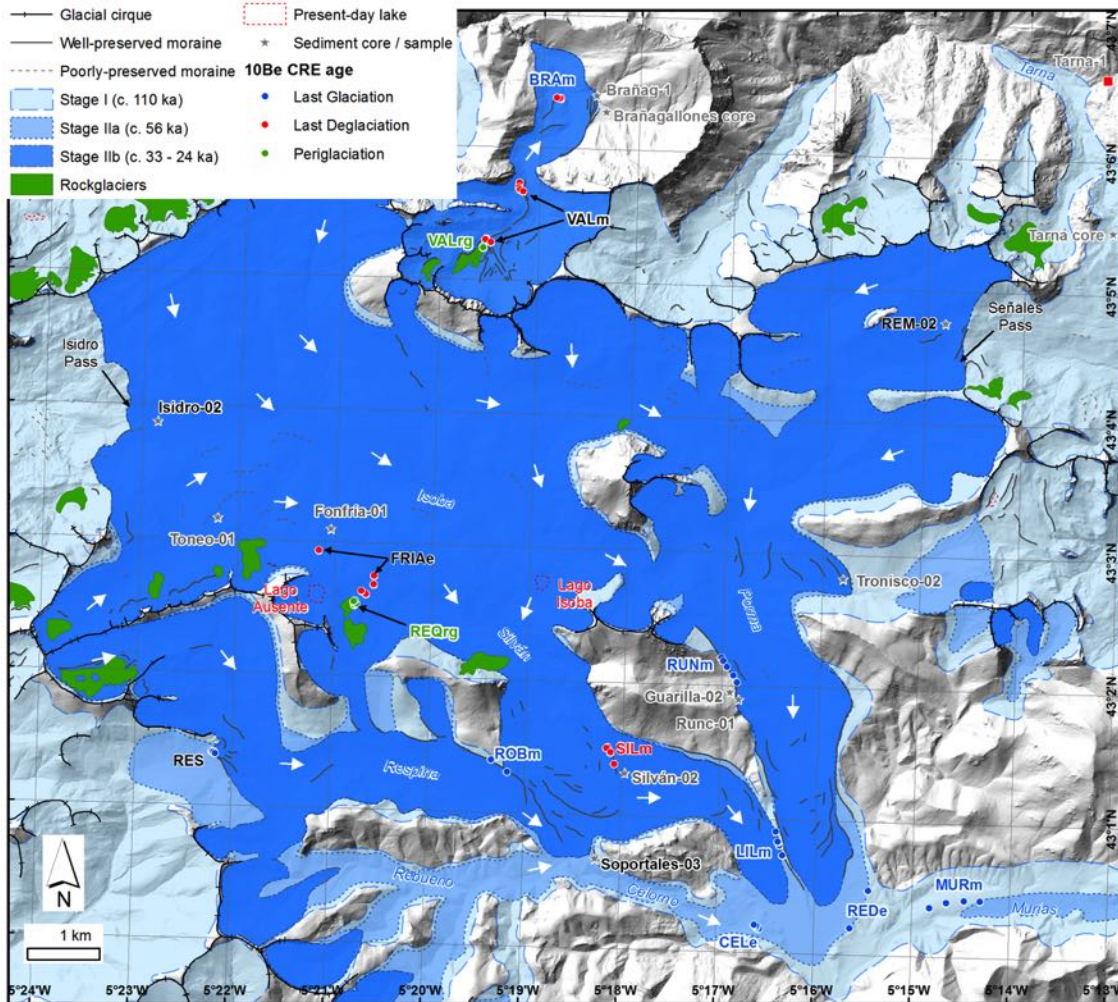
Figure 9.- Glacial stages and sample site locations of available [10]Be CRE, radiocarbon, and OSL ages in the Porma and Monasterio valleys (white arrows indicate ice flow directions). [10]Be CRE dataset is classified in: Last Glaciation (blue); Last Deglaciation (red); and Periglaciation (green) [lowercase letter next to landform acronym indicates the type of boulder: m- moraine; e- erratic; rg- rock glacier]. The probability density

389 functions of [10]Be CRE results are provided by mountain slopes following the same color key (grey curves
390 represent [10]Be CRE ages of individual boulders).

391 **4.3. Comparisons with other continental and marine paleoclimate records**

392 The new set of numerical ages presented here supports long-standing glacial conditions in

393 the central Cantabrian Mountains from ~56 to 22 ka (Glacial Stages IIa to IIb) spanning MIS

394 3 to MIS 2. Similar evolution has been reported in other Atlantic settings like the British

395 Isles, glaciated prior to ~35–40 ka and during the LGM (culminating at ~26–21 ka) (Rolfe et

396 al., 2012); or the Marrakech High Atlas, extensively glaciated from ~50.2 ka to 22 ka

397 (Hughes et al., 2018). Remarkable glacier oscillations through MIS 3 before the LGM have

398 been also documented in multiple mountain settings across the Mediterranean, like

399 Peloponnesus in Greece (~40–30 ka; Pope et al., 2015) or Mount Akdağ in SW Turkey (~31.5

400 ka; Sarikaya et al., 2014). Burial ages from the Monasterio and Porma moraines suggest that

401 the local LGM advance occurred between 33 and 24 ka, consistently with the new LGM

402 definition proposed by Hughes and Gibbard (2015). Meanwhile, [10]Be CRE ages obtained

403 from the lateral moraines indicate that glacier recession started at ~21–20 ka, after the LGM.

404 This pattern is time consistent with the growth of continental ice sheets to their maximum

405 positions between 33 and 26.5 ka, and their subsequent retreat due to a rise of northern

406 summer insolation between 20–19 ka (Clark et al., 2009). The close synchronicity between

407 Greenland coolest temperatures and the insolation minima at c. 24 ka BP suggests the strong

408 northern-insolation control of Ice-Age Cycles (Alley et al., 2002).

409 Mountain glaciers in central Spain reached their maximum areal extent at 26.1 ± 1.3 ka in

410 response to a period of rainfall increase (from 25 to 29 ka) under insolation minima

411 conditions (Domínguez-Villar et al., 2013). The available framework of numerical ages in

412 the Pyrenees suggests that more extensive glacier re-advances occurred during MIS 2 in the

413   Mediterranean influenced end of the range compared to the Atlantic influenced end of the

414   range (Delmas, 2015). This pattern could probably be related to a more active Balearic low

415   atmospheric pressure (Calvet et al., 2011). Iberian mountain glacier growth during MIS 2

416   was favored by the occurrence of relatively cold and humid conditions, as indicated in

417   lacustrine records from the Iberian Peninsula that show periods of positive hydrological

418   balance linked to reduced summer insolation (Moreno et al., 2012).

419   Marine records indicate that the Polar Front did not migrate as far south as the Iberian Margin

420   during the LGM (Eynaud et al., 2009) and Sea Surface Temperature (SST) cooled only

421   slightly down (1–2ºC temperature difference) reaching average Holocene temperature

422   (Sánchez Goñi et al., 2008). In contrast, massive iceberg calving caused more pronounced

423   southward shifts of the Polar Front during Heinrich Stadials than during the LGM, reaching

424   as far south as 40ºN latitude during HS1 (15.9 to 18.3 cal ka BP) (Eynaud et al., 2009).

425   Continental ice sheet collapses during Termination 1 resulted in massive meltwater and

426   iceberg discharge into the North Atlantic Ocean (Toucanne et al., 2015), perturbing the

427   northern overturning circulation and causing global changes in ocean and atmospheric

428   circulation patterns (Denton et al., 2010). Particularly, the southward shift of the Polar Front

429   during HS1 and the extensive sea ice coverage prevented the readvance of the southern

430   Scandinavian Ice Sheet margin due to moisture starvation (Rinterknecht, 2006). The

431   extremely cold and arid conditions (winter signature) that prevailed during HS1 in the North

432   Atlantic region due to extensive winter sea ice formation seem to have also forced the Iberian

433   Mountain glaciers to reduce their areal extent in response to moisture starvation.

434   **5. Conclusions**

435   Multi-dating approaches are the best options to provide a detailed view of mountain glacier

436   evolution and identify potential age conflicts between numerical ages derived from the

437   different techniques. Combined or alone, the results of the three techniques applied in the

438   Porma basin highlight the importance of: (i) developing statistical CRE analysis of multiple

439   boulders from the same landform (preferably more than 3 boulders per landform); (ii)

440   working preferentially with plant macro remain samples or pollen concentrates to avoid

441   radiocarbon aging effects; and (iii) giving priority to the water-transported sediments (glacio-

442   fluvial and alluvial) that show the longest travel distances to minimize cases of quartz

443   saturated OSL signals.

444   The glacial sequence preserved in the Porma valley, southern slope of the central Cantabrian

445   Mountains, provides consistent evidence that glaciers oscillated at various times throughout

446   the Last Glacial Cycle (from MIS 5d to MIS 2). Diachronous ^{10}Be CRE ages in lateral

447   moraines match the age of erratic and moraines boulders from the terminal zone, suggesting

448   that deposition of lateral moraines took long periods of time or even occurred during several

449   glacial stages. The combination of ^{10}Be CRE ages with other dating techniques (radiocarbon

450   and OSL) applied to moraine, and kame terraces suggest glacial occupation through MIS 3

451   (Stage IIa: ~56 ka) and MIS 2 (Stages IIb: ~ 33–24 ka). Numerical ages support a significant

452   advance of glaciers in the central Cantabrian Mountains during MIS 2 (33–24 ka) in response

453   to rainfall increases under cooling conditions related to insolation minima. Glacier retreat

454   started at ~ 21–20 ka due to orbital forcing and continued during HS1 as consequence

455   moisture scarcity under hyper-cool conditions due to iceberg and meltwater discharges in the

456   North Atlantic Region. Like in the western end of the Pyrenees, the advance of glaciers

457   during MIS 2 recorded inward glacier front positions respect to the local Pleistocene glacial

458   maximum in the southern slope of the Cantabrian Mountains. Further studies from other

459   Cantabrian valleys are required to draw more detailed conclusions about differences in

460   atmospheric circulation patterns between the Atlantic and Mediterranean domains.

35

Author contributions

Samples for surface exposure dating were taken in the field by LRR, MJDC, MJS and VR. ^{10}Be targets were prepared at the *Laboratoire National des Nucleides Cosmogéniques* (LN2C-CNRS) by LL. The isotopic ratio ^{10}Be/^{9}Be was measured at the ASTER AMS facility (CEREGE) by the ASTER Team [GA, KK, and DB]. Exposure ages were calculated and interpreted by LRR and VR. Sediment cores were drilled in the field by LRR, SGL, DB, MJDC, MJS and PV. Detailed laboratory descriptions and sampling for radiocarbon dating were done by LRR and SGL. OSL samples were taken in the field by SGL, LRR, DB and MJDC, while lab processing and age estimations were done by JS. The paper was written by LRR and all coauthors contributed to the discussion.

Acknowledgements

485 **References**
486

487 AKÇAR, N., YAVUZ, V., IVY-OCHS, S., REBER, R., KUBIK, P. W., ZAHNO, C. &
488   SCHLÜCHTER, C. 2014. Glacier response to the change in atmospheric circulation
489   in the eastern Mediterranean during the Last Glacial Maximum. *Quaternary*
490   *Geochronology,* 19**,** 27-41.

491 ALLEY, R. B., BROOK, E. J. & ANANDAKRISHNAN, S. 2002. A northern lead in the
492   orbital band: north-south phasing of Ice-Age Events. *Quaternary Science Reviews,*
493   21**,** 431-441.

494 ARNOLD, M., MERCHEL, S., BOURLÈS, D., BRAUCHER, R., BENEDETTI, L.,
495   FINKEL, R. C., AUMAÎTRE, G., GOTTDANG, A. & KLEIN, M. 2010. The French
496   accelerator mass spectrometry facility ASTER: Improved performance and
497   developments. *Nuclear Instruments and Methods in Physics Research B,* 268**,** 1954-
498   1959.

499 BALCO, G. 2006. Converting Al and Be isotope ratio measurements to nuclide
500   concentrations in quartz. Available from: https:// hess.ess.washington.edu.

501 BALCO, G., STONE, J. O., LIFTON, N. A. & DUNAI, T. J. 2008. A complete and easily
502   accessible means of calculating surface exposure ages or erosion rates from 10Be and
503   26Al measurements. *Quaternary Geochronology,* 3**,** 174-195.

504 BARROIS, C. 1882. *Recherches sur les terrains anciens des Asturies et de la Galice,* Lille,
505   Six-Horemans.

506 BORCHERS, B., MARRERO, S., BALCO, G., CAFFEE, M., GOEHRING, B., LIFTON,
507   N., NISHIIZUMI, K., PHILLIPS, F., SCHAEFER, J. & STONE, J. 2016. Geological
508   calibration of spallation production rates in the CRONUS-Earth project. *Quaternary*
509   *Geochronology,* 31**,** 188-198.

510 BRAUCHER, R., GUILLOU, V., BOURLÈS, D. L., ARNOLD, M., AUMAÎTRE, G.,
511   KEDDADOUCHE, K. & NOTTOLI, E. 2015. Preparation of ASTER in-house 10
512   Be/ 9 Be standard solutions. *Nuclear Instruments and Methods in Physics Research*
513   *Section B: Beam Interactions with Materials and Atoms,* 361**,** 335-340.

514 CALVET, M. 2012. Unravelling the last glaciation in the Pyrenees : an overview of recent
515   advances. *Quaternary International,* 279-280**,** 78.

516 CALVET, M., DELMAS, M., GUNNELL, Y., BRAUCHER, R. & BOURLÈS, D. 2011.
517   Recent Advances in Research on Quaternary Glaciations in the Pyrenees. *In:*
518   EHLERS, J., GIBBARD, P. & HUGHES, P. (eds.) *Developments in Quaternary*
519   *Science.* Amsterdam: Elsevier.

520 CARRASCO, R. M., PEDRAZA, J., DOMÍNGUEZ-VILLAR, D., WILLENBRING, J. K.
521 & VILLA, J. 2015. Sequence and chronology of the Cuerpo de Hombre paleoglacier
522 (Iberian Central System) during the last glacial cycle. *Quaternary Science Reviews,*
523 129**,** 163-177.

524 CARRASCO, R. M., VILLA, J. D. L., PEDRAZA GILSANZ, J. D., DOMINGUEZ-
525 VILLAR, D. & WILLENBRING, J. K. 2011. Reconstrucción y cronología del glaciar
526 de meseta de la Sierra de Béjar (Sistema Central Español) durante el máximo glaciar.
527 *Boletín de la Real Sociedad Española de Historia Natural. Sección Geológica,* 105**,**
528 125-135.

529 CHMELEFF, J., VON BLANCKENBURG, F., KOSSERT, K. & JAKOB, D. 2010.
530 Determination of the 10Be half-life by multicollector ICP-MS and liquid scintillation
531 counting. *Nuclear Instruments and Methods in Physics Research Section B: Beam*
532 *Interactions with Materials and Atoms,* 268**,** 192-199.

533 CLARK, P. U., DYKE, A. S., SHAKUN, J. D., CARLSON, A. E., CLARK, J.,
534 WOHLFARTH, B., MITROVICA, J. X., HOSTETLER, S. W. & MCCABE, A. M.
535 2009. The Last Glacial Maximum. *Science,* 325**,** 710-714.

536 DEHNERT, A., PREUSSER, F., KRAMERS, J. D., AKCAR, N., KUBIK, P. W., REBER,
537 R. & SCHLUECHTER, C. 2010. A multi-dating approach applied to proglacial
538 sediments attributed to the Most Extensive Glaciation of the Swiss Alps. *Boreas,* 39**,**
539 620-632.

540 DELMAS, M. 2015. The last maximum ice extent and subsequent deglaciation of the
541 Pyrenees: an overview of recent research. *Cuadernos de Investigación Geográfica,*
542 41**,** 359.

543 DELMAS, M., CALVET, M., GUNNELL, Y., BRAUCHER, R. & BOURLÈS, D. 2011.
544 Palaeogeography and 10Be exposure-age chronology of Middle and Late Pleistocene
545 glacier systems in the northern Pyrenees: Implications for reconstructing regional
546 palaeoclimates. *Palaeogeography, Palaeoclimatology, Palaeoecology,* 305**,** 109-122.

547 DELMAS, M., GUNNELL, Y., BRAUCHER, R., CALVET, M. & BOURLÈS, D. 2008.
548 Exposure age chronology of the last glaciation in the eastern Pyrenees. *Quaternary*
549 *Research,* 69**,** 231-241.

550 DELUNEL, R., BOURLÈS, D. L., VAN DER BEEK, P. A., SCHLUNEGGER, F., LEYA,
551 I., MASARIK, J. & PAQUET, E. 2014. Snow shielding factors for cosmogenic
552 nuclide dating inferred from long-term neutron detector monitoring. *Quaternary*
553 *Geochronology,* 24**,** 16-26.

554   DENTON, G., ANDERSON, R., TOGGWEILER, J., EDWARDS, R., SCHAEFER, J. &
555   PUTNAM, A. 2010. The last glacial termination. *Science,* 328**,** 1652-1656.

556   DOMÍNGUEZ-VILLAR, D., CARRASCO, R., PEDRAZA, J., CHENG, H., EDWARDS,
557   R. & WILLENBRING, J. 2013. Early maximum extent of paleoglaciers from
558   Mediterranean mountains during the last glaciation. *Scientific Reports,* 3.

559   EYNAUD, F., DE ABREU, L., VOELKER, A., SCHÖNFELD, J., SALGUEIRO, E.,
560   TURON, J.-L., PENAUD, A., TOUCANNE, S., NAUGHTON, F., SÁNCHEZ
561   GOÑI, M. F., MALAIZÉ, B. & CACHO, I. 2009. Position of the Polar Front along
562   the western Iberian margin during key cold episodes of the last 45 ka. *Geochemistry,*
563   *Geophysics, Geosystems,* 10**,** n/a-n/a.

564   FOMBELLA-BLANCO, M. A., GARCÍA-ROVÉS, E. & PUENTE-GARCÍA, E. 2003.
565   Comparative palynological analysis between the San Isidro and Leitariegos Holocene
566   sequences, NW Spain. *Acta Paleontologica Sinica,* 42**,** 111-117.

567   FOMBELLA-BLANCO, M. A., GARCÍA-ROVÉS, E. & PUENTE-GARCÍA, E.
568   Environmental and climatic changes inferred from the pollen sequence of San Isidro,
569   León, NW Spain. XI International Palynological Congress, 2004. Córdoba: Servicio
570   de publicaciones Universidad de Córdoba, 483-484.

571   FROCHOSO, M., GONZÁLEZ-PELLEJERO, R. & ALLENDE, F. 2013. Pleistocene glacial
572   morphology and timing of last glacial cycle in cantabrian mountains (Northern
573   Spain): new chronological data from the Asón area. *Open Geosciences,* 5.

574   GALBRAITH, R. F., ROBERTS, R. G., LASLETT, G. M., YOSHIDA, H. & OLLEY, J. M.
575   1999. Optical dating of single grains of quartz from Jinmium rock shelter, northern
576   Australia. Part I: experimental design and statistical models. *Archaeometry,* 41**,** 339-
577   364.

578   GIRAUDI, C., BODRATO, G., LUCCHI, M. R., CIPRIANI, N., VILLA, I. M., GIACCIO,
579   B. & ZUPPI, G. M. 2011. Middle and late Pleistocene glaciations in the Campo Felice
580   Basin (central Apennines, Italy). *Quaternary Research,* 75**,** 219-230.

581   GUERIN, G., MERCIER, N. & ADAMIEC, G. 2011. Dose-rate conversion factors: update.
582   *Ancient TL,* 29.

583   HEYMAN, J., APPLEGATE, P. J., BLOMDIN, R., GRIBENSKI, N., HARBOR, J. M. &
584   STROEVEN, A. P. 2016. Boulder height – exposure age relationships from a global
585   glacial 10Be compilation. *Quaternary Geochronology,* 34**,** 1-11.

586　HEYMAN, J., STROEVEN, A. P., HARBOR, J. M. & CAFFEE, M. W. 2011. Too young
587　　　　or too old: Evaluating cosmogenic exposure dating based on an analysis of compiled
588　　　　boulder exposure ages. *Earth and Planetary Science Letters,* 302**,** 71-80.

589　HUGHES, P., WOODWARD, J., GIBBARD, P., MACKLIN, M., GILMOUR, M. &
590　　　　SMITH, G. 2006. The glacial history of the Pindus Mountains, Greece. *The Journal*
591　　　　*of geology,* 114**,** 413-434.

592　HUGHES, P. D., FINK, D., RODÉS, Á., FENTON, C. R. & FUJIOKA, T. 2018. Timing of
593　　　　Pleistocene glaciations in the High Atlas, Morocco: New 10 Be and 36 Cl exposure
594　　　　ages. *Quaternary Science Reviews,* 180**,** 193-213.

595　HUGHES, P. D. & GIBBARD, P. L. 2015. A stratigraphical basis for the Last Glacial
596　　　　Maximum (LGM). *Quaternary International,* 383**,** 174-185.

597　HUGHES, P. D., GIBBARD, P. L. & EHLERS, J. 2013. Timing of glaciation during the last
598　　　　glacial cycle: evaluating the concept of a global 'Last Glacial Maximum' (LGM).
599　　　　*Earth-Science Reviews,* 125**,** 171-198.

600　HUGHES, P. D. & WOODWARD, J. C. 2008. Timing of glaciation in the Mediterranean
601　　　　mountains during the last cold stage. *Journal of Quaternary Science,* 23**,** 575-588.

602　HUGHES, P. D., WOODWARD, J. C., VAN CALSTEREN, P. C., THOMAS, L. E. &
603　　　　ADAMSON, K. R. 2010. Pleistocene ice caps on the coastal mountains of the
604　　　　Adriatic Sea. *Quaternary Science Reviews,* 29**,** 3690-3708.

605　IVY-OCHS, S., KERSCHNER, H., REUTHER, A., PREUSSER, F., HEINE, K., MAISCH,
606　　　　M., KUBIK, P. W. & SCHLÜCHTER, C. 2008. Chronology of the last glacial cycle
607　　　　in the European Alps. *Journal of Quaternary Science,* 23**,** 559-573.

608　JALUT, G., TURU I MICHELS, V., DEDOUBAT, J.-J., OTTO, T., EZQUERRA, J.,
609　　　　FONTUGNE, M., BELET, J. M., BONNET, L., DE CELIS, A. G., REDONDO-
610　　　　VEGA, J. M., VIDAL-ROMANÍ, J. R. & SANTOS, L. 2010. Palaeoenvironmental
611　　　　studies in NW Iberia (Cantabrian range): Vegetation history and synthetic approach
612　　　　of the last deglaciation phases in the western Mediterranean. *Palaeogeography,*
613　　　　*Palaeoclimatology, Palaeoecology,* 297**,** 330-350.

614　JIMÉNEZ-SÁNCHEZ, M. & FARIAS-ARQUER, P. 2002. New radiometric and
615　　　　geomorphologic evidences of a last glacial maximum older than 18 ka in SW
616　　　　European mountains: the example of Redes Natural Park (Cantabrian Mountains, NW
617　　　　Spain). *Geodinamica Acta,* 15**,** 93-101.

618　JIMÉNEZ-SÁNCHEZ, M., RODRÍGUEZ-RODRÍGUEZ, L., GARCÍA-RUIZ, J. M.,
619　　　　DOMÍNGUEZ-CUESTA, M. J., FARIAS, P., VALERO-GARCÉS, B., MORENO,

620   A., RICO, M. & VALCÁRCEL, M. 2013. A review of glacial geomorphology and
621   chronology in northern Spain: Timing and regional variability during the last glacial
622   cycle. *Geomorphology,* 196**,** 50-64.

623   JULL, A. J. T., BURR, G. S. & HODGINS, G. W. L. 2013. Radiocarbon dating, reservoir
624   effects, and calibration. *Quaternary International,* 299**,** 64-71.

625   KLASEN, N., FIEBIG, M., PREUSSER, F., REITNER, J. M. & RADTKE, U. 2007.
626   Luminescence dating of proglacial sediments from the Eastern Alps. *Quaternary*
627   *International,* 164-165**,** 21-32.

628   KLEIN, M. G., GOTTDANG, A., MOUS, D. J. W., BOURLÈS, D. L., ARNOLD, M.,
629   HAMELIN, B., AUMAÎTRE, G., BRAUCHER, R., MERCHEL, S. & CHAUVET,
630   F. 2008. Performance of the HVE 5MV AMS system at CEREGE using an absorber
631   foil for isobar suppression. *Nuclear Instruments and Methods in Physics Research*
632   *Section B: Beam Interactions with Materials and Atoms,* 266**,** 1828-1832.

633   KOHL, C. & NISHIIZUMI, K. 1992. Chemical isolation of quartz for measurement of in-
634   situ-produced cosmogenic nuclides. *Geochimica et Cosmochimica Acta,* 56**,** 3583-
635   3587.

636   KORSCHINEK, G., BERGMAIER, A., FAESTERMANN, T., GERSTMANN, U. C.,
637   KNIE, K., RUGEL, G., WALLNER, A., DILLMANN, I., DOLLINGER, G., VON
638   GOSTOMSKI, C. L., KOSSERT, K., MAITI, M., POUTIVTSEV, M. &
639   REMMERT, A. 2010. A new value for the half-life of 10Be by Heavy-Ion Elastic
640   Recoil Detection and liquid scintillation counting. *Nuclear Instruments and Methods*
641   *in Physics Research Section B: Beam Interactions with Materials and Atoms,* 268**,**
642   187-191.

643   LAL, D. 1991. Cosmic ray labeling of erosion surfaces: in situ nuclide production rates and
644   erosion models. *Earth and Planetary Science Letters,* 104**,** 424-439.

645   MAKOS, M., RINTERKNECHT, V., BRAUCHER, R., TOŁOCZKO-PASEK, A.,
646   ARNOLD, M., AUMAÎTRE, G., BOURLÈS, D. & KEDDADOUCHE, K. 2018.
647   Last Glacial Maximum and Lateglacial in the Polish High Tatra Mountains- Revised
648   deglaciation chronology based on the 10Be exposure age dating. *Quaternary Science*
649   *Reviews,* 187**,** 130-156.

650   MERCHEL, S., ARNOLD, M., AUMAÎTRE, G., BENEDETTI, L., BOURLÈS, D.L.,
651   BRAUCHER, R., ALFIMOV, V., FREEMAN, S.P.H.T., STEIER, P., WALLNER,
652   A. 2008. Towards more precise 10Be and 36Cl data from measurements at the 10-14
653   level: influence of sample preparation. *Nuclear Instruments and Methods in Physics*
654   *Research Section B,* 266**,** 4921–4926.

655 MORENO, A., GONZÁLEZ-SAMPÉRIZ, P., MORELLÓN, M., VALERO-GARCÉS, B.
656   L. & FLETCHER, W. J. 2012. Northern Iberian abrupt climate change dynamics
657   during the last glacial cycle: A view from lacustrine sediments. *Quaternary Science*
658   *Reviews,* 36**,** 139-153.

659 MURRAY, A. & WINTLE, A. G. 2000. Luminescence dating of quartz using an improved
660   single-aliquot regenerative-dose protocol. *Radiation Measurements,* 32**,** 57-73.

661 NISHIIZUMI, K., IMAMURA, M., CAFFEE, M. W., SOUTHON, J. R., FINKEL, R. C. &
662   MCANINCH, J. 2007. Absolute calibration of [10]Be AMS standards. *Nuclear*
663   *Instruments and Methods in Physics Research Section B: Beam Interactions with*
664   *Materials and Atoms,* 258**,** 403-413.

665 PALACIOS, D., ANDRÉS, N., MARCOS, J. & VÁZQUEZ-SELEM, L. 2012a. Maximum
666   glacial advance and deglaciation of the Pinar Valley (Sierra de Gredos, Central Spain)
667   and its significance in the Mediterranean context. *Geomorphology,* 177-178**,** 51-61.

668 PALACIOS, D., DE ANDRÉS, N., DE MARCOS, J. & VÁZQUEZ-SELEM, L. 2012b.
669   Glacial landforms and their paleoclimatic significance in Sierra de Guadarrama,
670   Central Iberian Peninsula. *Geomorphology,* 139-140**,** 67-78.

671 PALACIOS, D., DE MARCOS, J. & VÁZQUEZ-SELEM, L. 2011. Last Glacial Maximum
672   and deglaciation of Sierra de Gredos, central Iberian Peninsula. *Quaternary*
673   *International,* 233**,** 16-26.

674 PALACIOS, D., GÓMEZ-ORTIZ, A., ANDRÉS, N., VÁZQUEZ-SELEM, L.,
675   SALVADOR-FRANCH, F. & OLIVA, M. 2015. Maximum extent of Late
676   Pleistocene glaciers and last deglaciation of La Cerdanya mountains, Southeastern
677   Pyrenees. *Geomorphology,* 231**,** 116-129.

678 PALLÀS, R., RODÉS, Á., BRAUCHER, R., BOURLÈS, D., DELMAS, M., CALVET, M.
679   & GUNNELL, Y. 2010. Small, isolated glacial catchments as priority targets for
680   cosmogenic surface exposure dating of Pleistocene climate fluctuations, southeastern
681   Pyrenees. *Geology,* 38**,** 891-894.

682 PALLÀS, R., RODÉS, Á., BRAUCHER, R., CARCAILLET, J., ORTUÑO, M.,
683   BORDONAU, J., BOURLÈS, D., VILAPLANA, J. M., MASANA, E. &
684   SANTANACH, P. 2006. Late Pleistocene and Holocene glaciation in the Pyrenees:
685   a critical review and new evidence from 10Be exposure ages, south-central Pyrenees.
686   *Quaternary Science Reviews,* 25**,** 2937-2963.

687 PRESCOTT, R. & HUTTON, J. 1994. Cosmic ray contributions to dose rates for
688   luminescence and ESR dating: Large depths and long term time variations. *Radiation*
689   *Measurements,* 23**,** 497-500.

690 REIMER, P., BARD, E., BAYLISS, A., BECK, J. W., BLACKWELL, P., RAMSEY, C. B.,
691   BUCK, C., CHENG, H., EDWARDS, R. L., FRIEDRICH, M., GROOTES, P. M.,
692   GUILDERSON, T. P., HAFLIDASON, H., HAJDAS, I., HATTÉ, C., HEATON, T.
693   J., HOFFMANN, D. L., HOGG, A. G., HUGHEN, K., KAISER, K. F., KROMER,
694   B., MANNING, S. W., NIU, M., REIMER, R. W., RICHARDS, D. A., SCOTT, E.
695   M., SOUTHON, J., STAFF, R. A., TURNEY, C. S. M. & VAN DER PLICHT, J.
696   2013. Intcal13 and Marine13 radiocarbon age calibration curves 0-50,000 years cal
697   BP. *Radiocarbon,* 55**,** 1869-1887.

698 RINTERKNECHT, V. R. 2006. The Last Deglaciation of the Southeastern Sector of the
699   Scandinavian Ice Sheet. *Science,* 311**,** 1449-1452.

700 RIXHON, G., BRIANT, R. M., CORDIER, S., DUVAL, M., JONES, A. & SCHOLZ, D.
701   2017. Revealing the pace of river landscape evolution during the Quaternary: recent
702   developments in numerical dating methods. *Quaternary Science Reviews,* 166**,** 91-
703   113.

704 RODRÍGUEZ-RODRÍGUEZ, L., JIMÉNEZ-SÁNCHEZ, M., DOMÍNGUEZ-CUESTA, M.
705   J. & ARANBURU, A. 2015. Research history on glacial geomorphology and
706   geochronology of the Cantabrian Mountains, north Iberia (43–42°N/7–2°W).
707   *Quaternary International,* 364**,** 6-21.

708 RODRÍGUEZ-RODRÍGUEZ, L., JIMÉNEZ-SÁNCHEZ, M., DOMÍNGUEZ-CUESTA, M.
709   J., RINTERKNECHT, V., PALLÀS, R., AUMAÎTRE, G., BOURLÈS, D. L. &
710   KEDDADOUCHE, K. 2017. Timing of last deglaciation in the Cantabrian Mountains
711   (Iberian Peninsula; North Atlantic Region) based on in situ-produced [10]Be exposure
712   dating. *Quaternary Science Reviews,* 171**,** 166-181.

713 RODRÍGUEZ-RODRÍGUEZ, L., JIMÉNEZ-SÁNCHEZ, M., DOMÍNGUEZ-CUESTA, M.
714   J., RINTERKNECHT, V., PALLÀS, R. & BOURLÈS, D. 2016. Chronology of
715   glaciations in the Cantabrian Mountains (NW Iberia) during the Last Glacial Cycle
716   based on in situ-produced [10]Be. *Quaternary Science Reviews,* 138**,** 31-48.

717 RODRÍGUEZ-RODRÍGUEZ, L., JIMÉNEZ-SÁNCHEZ, M., DOMÍNGUEZ-CUESTA, M.
718   J., RINTERKNECHT, V., PALLÀS, R., BOURLÈS, D. & VALERO-GARCÉS, B.
719   2014. A multiple dating-method approach applied to the Sanabria Lake moraine
720   complex (NW Iberian Peninsula, SW Europe). *Quaternary Science Reviews,* 83**,** 1-
721   10.

722 ROLFE, C. J., HUGHES, P. D., FENTON, C. R., SCHNABEL, C., XU, S. & BROWN, A.
723   G. 2012. Paired 26Al and 10Be exposure ages from Lundy: new evidence for the
724   extent and timing of Devensian glaciation in the southern British Isles. *Quaternary*
725   *Science Reviews,* 43**,** 61-73.

726 RUIZ-FERNÁNDEZ, J., OLIVA, M., CRUCES, A., LOPES, V., FREITAS, M. D. C.,
727   ANDRADE, C., GARCÍA-HERNÁNDEZ, C., LÓPEZ-SÁEZ, J. A. & GERALDES,
728   M. 2016. Environmental evolution in the Picos de Europa (Cantabrian Mountains,
729   SW Europe) since the Last Glaciation. *Quaternary Science Reviews,* 138**,** 87-104.

730 SÁNCHEZ GOÑI, M. F., LANDAIS, A., FLETCHER, W. J., NAUGHTON, F., DESPRAT,
731   S. & DUPRAT, J. 2008. Contrasting impacts of Dansgaard–Oeschger events over a
732   western European latitudinal transect modulated by orbital parameters. *Quaternary*
733   *Science Reviews,* 27**,** 1136-1151.

734 SARIKAYA, M. A., ÇINER, A., HAYBAT, H. & ZREDA, M. 2014. An early advance of
735   glaciers on Mount Akdağ, SW Turkey, before the global Last Glacial Maximum;
736   insights from cosmogenic nuclides and glacier modeling. *Quaternary Science*
737   *Reviews,* 88**,** 96-109.

738 SCHILDGEN, T. F., PHILLIPS, W. M. & PURVES, R. S. 2005. Simulation of snow
739   shielding corrections for cosmogenic nuclide surface exposure studies.
740   *Geomorphology,* 64**,** 67-85.

741 SERRANO, E., GONZÁLEZ-TRUEBA, J. J. & GONZÁLEZ-GARCÍA, M. 2012. Mountain
742   glaciation and paleoclimate reconstruction in the Picos de Europa (Iberian Peninsula,
743   SW Europe). *Quaternary Research,* 78**,** 303-314.

744 SERRANO, E., GONZÁLEZ-TRUEBA, J. J., PELLITERO, R., GONZÁLEZ-GARCÍA, M.
745   & GÓMEZ-LENDE, M. 2013. Quaternary glacial evolution in the Central Cantabrian
746   Mountains (Northern Spain). *Geomorphology,* 196**,** 65-82.

747 STOCKES, S. 1999. Luminescence dating applications in geomorphological research.
748   *Geomorphology,* 29**,** 153-171.

749 STONE, J. 2000. Air pressure and cosmogenic isotope production. *Journal of Geophysical*
750   *Research,* 105**,** 23753-23759.

751 STUIVER, M. & REIMER, P. J. 1993. Extended ^{14}C data base and revised CALIB 3.0 [14]C
752   age calibration program. *Radiocarbon,* 35**,** 215-230.

753 TOUCANNE, S., SOULET, G., FRESLON, N., JACINTO, R. S., DENNIELOU, B.,
754   ZARAGOSI, S., EYNAUD, F., BOURILLET, J. F. & BAYON, G. 2015. Millennial-
755   scale fluctuations of the European Ice Sheet at the end of the last glacial, and their
756   potential impact on global climate. *Quaternary Science Reviews,* 123**,** 113-133.

757 VIDAL ROMANÍ, J., FERNÁNDEZ MOSQUERA, D., MARTI, K. & BRUM-FERREIRA,
758   A. 1999. Nuevos datos para la cronología glaciar pleistocena en el NW de la
759   Península Ibérica. *Cuadernos Laboratorio Xeolóxico de Laxe,* 24**,** 7-29.

760 WINTLE, A. G. & MURRAY, A. S. 2006. A review of quartz optically stimulated
761   luminescence characteristics and their relevance in single-aliquot regeneration dating
762   protocols. *Radiation Measurements,* 41**,** 369-391.

763 WOODWARD, J. C. & HUGHES, P. D. 2011. Glaciation in Greece: A New Record of Cold
764   Stage Environments in the Mediterranean. *In:* EHLERS, J., GIBBARD, P. &
765   HUGHES, P. D. (eds.) *Developments in Quaternary Science.* Amsterdam: Elsevier.

766 ZWECK, C., ZREDA, M. & DESILETS, D. 2013. Snow shielding factors for cosmogenic
767   nuclide dating inferred from Monte Carlo neutron transport simulations. *Earth and*
768   *Planetary Science Letters,* 379**,** 64-71.
769